NASA Technical Memorandum 80059

NASA-TM-80059 19790018710

AN EVALUATION OF LINEAR ACOUSTIC THEORY FOR A HOVERING ROTOR

C. E. K. Morris, Jr.; F. Farassat; and
P. A. Nystrom

May 1979

National Aeronautics and
Space Administration
Langley Research Center
Hampton, Virginia 23665

1 Report No	2 Government Accession No	3 Recipient's Catalog No
NASA TM 80059		

4 Title and Subtitle	5 Report Date
An Evaluation of Linear Acoustic Theory for a Hovering Rotor	May 1979
	6 Performing Organization Code

7 Author(s)	8 Performing Organization Report No
C. E. K. Morris, Jr.; F. Farassat;* and P. A. Nystrom	
	10 Work Unit No
9 Performing Organization Name and Address	505-10-23-04
NASA Langley Research Center Hampton, Virginia 23665	11 Contract or Grant No
	13 Type of Report and Period Covered
12 Sponsoring Agency Name and Address	Technical Memorandum
National Aeronautics and Space Administration Washington, DC 20546	14 Sponsoring Agency Code

15 Supplementary Notes

*Joint Institute for Advancement of Flight Science

The work of F. Farassat was supported by the U. S. Army Research Office and NASA Grant NSG 1474. Acknowledgment: Special data supplied by Mr. D. A. Boxwell.

16 Abstract

Linear acoustic calculations are compared with previously reported data for a small-scale hovering rotor operated at high tip Mach numbers. The theoretical results were based on a detailed calculated description of the distributions of blade surface pressure and shear stress due to skin friction. The noise due to skin friction and loading, in the rotor disk plane, is found to be small compared to thickness noise. Thus the basic conclusions of Boxwell et al about the importance of nonlinear effects are upheld.

Some approximations involved in the current theories for the inclusion of nonlinear effects are discussed. Using a model nonlinear problem, it is shown that to use the acoustic analogy, good knowledge of the flowfield is required. Since the quadrupole noise calculation based on acoustic analogy involves extensive numerical work, it is argued that the results of linear acoustic theories should be corrected using an analytic approach which does not separate the aerodynamic and aeroacoustics problems.

17 Key Words (Suggested by Author(s))	18 Distribution Statement
Acoustics Rotor Blades Hover	Unclassified - Unlimited 71-Acoustics

19 Security Classif (of this report)	20 Security Classif (of this page)	21 No of Pages	22 Price*
Unclassified	Unclassified	56	$5.25

* For sale by the National Technical Information Service Springfield Virginia 22161

AN EVALUATION OF LINEAR ACOUSTIC THEORY FOR A HOVERING ROTOR

Charles E. K. Morris, Jr.
Langley Research Center

F. Farassat
Joint Institute for Advancement of Flight Sciences

Paul A. Nystrom
Langley Research Center

SUMMARY

Linear acoustic calculations are compared with previously reported data for a small-scale hovering rotor operated at high tip Mach numbers. The theoretical results were based on a detailed calculated description of the distributions of blade surface pressure and shear stress due to skin friction. The noise due to skin friction and loading, in the rotor disk plane, is found to be small compared to thickness noise. Thus, the basic conclusions of Boxwell, et al, about the importance of nonlinear effects are upheld.

Some approximations involved in the current theories for the inclusion of nonlinear effects are discussed. Using a model nonlinear problem, it is shown that to use the acoustic analogy, good knowledge of the flowfield is required. Since the quadrupole noise calculation based on acoustic analogy involves extensive numerical work, it is argued that the results of linear acoustic theories should be corrected using an analytic approach which does not separate the aerodynamic and aeroacoustics problems.

INTRODUCTION

One of the current challenging problems of aeroacoustics is the prediction of the noise from high-speed propellers and helicopter rotors. In the last decade, many researchers have addressed this problem with the result that

understanding of the noise generation mechanisms involved has been substantially improved. It was natural that the first mathematical formulations of this problem be based on linear equations. Perhaps the most important contribution in this field, from which many of the current noise prediction techniques have evolved, is the paper by Ffowcs Williams and Hawkings (ref. 1). In this paper, using acoustic analogy, they derived the now famous Ffowcs Williams-Hawkings equation (FW-H eq.). As is well-known from the jet noise theory, the nonlinear effects associated with large flow velocities are relegated to a single term involving the Lighthill stress tensor. By dropping this term, the current linear acoustic formulations can all be shown to be equivalent to the solution of the resulting simplified FW-H equation.

Recently, several authors have found that linear acoustic calculations for propellers and rotors fail to agree well with data for cases with substantial amounts of transonic flow. The linear methods underpredict both the width and amplitude of the main pulses of blade-passage noise (refs. 2 and 3). The neglect of the effects of nonlinearities is blamed as the cause of the underpredictions. Incomplete aerodynamic input data are used in the applications of linear acoustic theory in the published literature. For example, from the study of the governing acoustic equation, one may show that the force due to skin friction and the component of the force along the blade chord due to surface pressure generate noise with peaks in the rotor plane. Because the aerodynamic input data for calculation of these effects are difficult to obtain, they are generally neglected.

The aim of this paper is to evaluate the linear theory by using reliable geometric and aerodynamic input data in linear acoustic calculations for comparison with recently available experimental data by Boxwell, Yu, and

Schmitz (ref. 4). These data were obtained from a hovering 1/7-scale model of a UH-1H rotor operated at tip Mach numbers ranging between 0.8 and 1.0. The linear acoustic calculations in the present paper are based on a formulation involving integrals over the blade surface with observer time differentiation before the far-field integral (ref. 5). The blade spanwise distribution of effective angle of attack is obtained with the prescribed-wake, hovering-rotor method of Langrebe (refs. 6, 7, and 8). The pressure and skin-friction distributions on the blades are obtained with the transonic airfoil-analysis program of Bauer, et al (refs. 9, 10, and 11).

The current efforts to study nonlinear effects are all based on the acoustic analogy. Some problems associated with application of the acoustic analogy are discussed by studying the sound from a pulsating sphere. The difficulties associated with the use of acoustic analogy indicate that a direct approach for the study of nonlinear effects using the perturbation technique for a simplified problem, such as the nonlifting rotor, may be more fruitful than using the acoustic analogy.

This report expands on the presentation of some of this work in reference 12.

SYMBOLS

A generalized flow parameter (see eq. (2))

a radius of sphere, m

C_p airfoil pressure coefficient $\dfrac{p - p_\infty}{\frac{1}{2}\rho V_\infty^2}$

C_T rotor thrust coefficient, $\dfrac{\text{rotor thrust}}{\pi R^2 \rho (\Omega R)^2}$

C_Q rotor torque coefficient, $\frac{\text{rotor torque}}{\pi R^3 \rho (\Omega R)^2}$

c speed of sound in undisturbed medium, m/sec; or airfoil chord, m

c_f airfoil skin-friction coefficient, $\frac{\text{viscous shear stress}}{\frac{1}{2}\rho v^2}$, N/m^2

c_ℓ airfoil section lift coefficient

ℓ_r force per unit area on a fluid in the observer direction, N/m^2

M_r Mach number in the radiation direction (see eq. (1))

M_t rotor tip Mach number, $\frac{\Omega R}{c}$

M_1 nonlinear first-order radial velocity, nondimensional (see eq. (C-11))

$\vec{n}$ local unit outward normal

P_1 nonlinear first-order acoustic pressure, nondimensional (see eq. (C-10))

p local static pressure at a point, N/m^2

p' acoustic pressure, N/m^2

R rotor radius, 1.045 m

r distance between source and observer, $|\vec{x}-\vec{y}|$, m; or distance from center of pulsating sphere, m.

$\vec{r}$ radiation vector, $\vec{x}-\vec{y}$

$\hat{r}_i$ unit vector along radiation direction, $\vec{r}/|\vec{r}|$

S blade surface area, m^2

s renormalization variable (see eq. (C-7))

T period of blade passage, sec

T_{ij} Lighthill stress tensor

$\vec{t}$ local unit tangent

t observer time

u_1 first order fluid velocity (see eq. (3)), m/sec

v_i local blade velocity

v_n local normal velocity on the blades

x airfoil chordwise coordinate, measured from leading to trailing edge, m

$\vec{x}$ observer position vector

$\vec{y}$ source position vector

α airfoil angle of attack (angle between chord line and airstream vector, degrees; or variable of eq. (5)

γ ratio of specific heats of the medium

$\delta(\ )$ Dirac delta function

δ_{ij} Kronecker delta

ε perturbation parameter (see eq. (2))

ρ mass density of air, kg/m^3

σ viscous blade-surface tangential stress

ϕ velocity potential

Ω rotor rotational speed, rad/sec

ω frequency of oscillation, Hz

Subscripts

0 undisturbed medium

t boundary layer transition

∞ freestream conditions

$[\ ]_{ret}$ retarded time

LINEAR ACOUSTIC THEORY AND AERODYNAMIC INPUT

Since the available experimental data are for a hovering rotor, a computer program already developed for high-speed propellers was used for linear acoustic calculations. The subsonic part of this computer program uses a solution of the FW-H equation in the following form (ref. 5). The acoustic pressure $p'(\vec{x},t)$ is given by

$$4\pi\, p'(\vec{x},t) = \frac{1}{c}\frac{\partial}{\partial t}\int_{\text{blades}} \left[\frac{\rho_o c v_n + \ell_r}{r|1-M_r|}\right]_{\text{ret}} dS + \int_{\text{blades}} \left[\frac{\ell_r}{r^2|1-M_r|}\right]_{\text{ret}} dS \qquad (1)$$

where $M_r = v_i \hat{r}_i/c$. Because the helical tip Mach number of the rotor is less than one, the Doppler term, $|1-M_r|^{-1}$ will not produce a singularity.

Equation (1) is valid in both near and far fields. To use this equation for numerical calculation, the blades are divided into small panels. For each panel, the retarded time is found first, and then the integrands in eq. (1) are evaluated. The force on the fluid, ℓ_i, must be known at this stage and is supplied by other means discussed below. The integrals in eq. (1) are approximated by discrete sums over all the panels, and the first integral is differentiated numerically to get the acoustic pressure $p'(\vec{x},t)$. At all these steps, the observer position $\vec{x}$ and time t are kept fixed. Varying t in a prescribed interval results in an acoustic pressure signature which is generally very smooth. The precise rotor geometry is accounted for in the acoustic computer program. The program is described by a flow chart in figure 1 and discussed in Appendix A.

The acoustic pressure described in equation (1) is treated as having several components. Thickness noise is the component described by the term involving v_n, the local normal velocity on the blade. At each point on the blade, the force on the fluid may be expressed as the vector sum $\vec{\ell} = p\vec{n} + \sigma\vec{t}$ where $\vec{n}$ and $\vec{t}$ are the unit outward normal and unit tangent (in the direction of blade motion) to the blade surface, respectively. The loading noise component of $p(\vec{x},t)$ is described by the term involving the surface pressure p in equation (1). Skin-friction noise is described by the term involving σ, shear stress on the blade surface. The distributions of σ and p are obtained by the combined use of several computer programs for aerodynamics.

Aerodynamic inputs for the acoustic methods were obtained with modified versions of existing computer programs for predicting aerodynamic characteristics for airfoils and hovering rotors (Appendix B). The manner in which the programs were coupled is shown schematically in figure 2. The required inputs for the hovering rotor program (ref. 6) include airfoil data tables, rotor geometry and test conditions. The key output is the spanwise distribution of effective angle of attack (as influenced by nonuniform downwash and three-dimensional flow). The computed angle of attack then serves as an input when the transonic airfoil program (ref. 10) is utilized to obtain detailed pressure and skin-friction distributions at a series of spanwise blade stations. These distributions yield the values of p and σ required for the acoustic program.

COMPARISON OF THEORETICAL AND EXPERIMENTAL RESULTS

Experimental data.- The experimental data used here are reported in reference 4 for a 1/7-scale model of a UH-1H rotor operated at high tip speeds and low disk loading. The two-bladed rotor was run in an anechoic room designed to reduce recirculation. The microphone was located in the rotor

plane 1.5 diameters (3.14 m) from the rotor center. Rotor geometry and test conditions are described in Tables I and II, respectively. A detailed description of the test facilities and measuring equipment are found in reference 4.

Aerodynamics.- Several steps preceded the utilization of the hovering rotor program of Landgrebe. First, a subcritical airfoil-analysis program (ref. 13) was used to guide the prediction of laminar-to-turbulent transition points for the airfoil boundary layer. The predicted transition characteristics, shown in figure 3, were required inputs for the transonic airfoil program. This latter program and the wind-tunnel data of reference 14 were used to construct airfoil-characteristics tables for the hovering rotor program. The airfoil lift characteristics, shown in figure 4, are for an NACA 0012 airfoil as influenced by the operating conditions of the test rotor of reference 4. (The portion of those tables actually used by the rotor program for the present report are indicated by the location of the curves of lift coefficient and Mach number calculated for three test conditions.)

Rotor geometry and test conditions (Tables I and II, respectively) were also required inputs for the prescribed-wake rotor program. Rotor rotational speed was adjusted to give tip Mach numbers ranging from 0.6 to 0.962 for a sonic speed of 340.3 m/sec. Fifteen lifting-line segments modeled each blade: five segments stretched from 0.144 to 0.8 radius, and ten segments, 0.02 radius wide, represented the remaining outboard end.

Some results of the rotor-program calculations are shown in figures 4, 5, and 6. The peaks of the data curves at the outboard blade region in figure 5 indicate the effect of tip-vortices on the local downwash velocity and, hence, on effective angle of attack. The influence of compressibility effects on drag rise is shown in figure 6. The high-speed regions at the blade tips produce most of the drag and require most of the power.

The transonic airfoil code was then used to calculate details of the blade-surface flow condition at fifteen spanwise positions for each tip speed. Angle-of-attack data, such as given in figure 5, transition values from figure 3, and calculated values of Reynolds and Mach numbers constituted the input list for each airfoil flow condition. All fifteen data sets required for one rotor tip-speed condition were obtained in one computer run.

Outputs from the transonic airfoil program were used in dimensional form by the acoustic program. A set of 30 data points was supplied for each blade section for pressure and for shear values. The first ten points were located in the first seven percent of the blade section. This distribution of points reflects attention given to requirements for adequate definition of contours under a wide range of conditions. Figure 7 shows details of the distributions of blade surface pressure, p, and shear stress, σ, for the sample case with 0.9 tip Mach number. (The pressure plots are staggered to the right and the shear stress are staggered obliquely to make each curve more easily distinguishable.) Trailing-edge oscillations for some σ curves are related to separation phenomena; they signify the breakdown of the boundary-layer model used in the computer program. These oscillations have a negligible effect on the acoustic calculations.

Aerodynamic predictions of the prescribed-wake and the acoustic programs are compared in figures 8 and 9. The acoustic program obtains these results by integrating both pressure and shear distributions on the blades, whereas the prescribed-wake program obtains its final results with airfoil tables and correction factors. Figure 8 shows that the two methods are in good agreement on spanwise loading, except for the tip at the highest tip speed. The

differences in rotor thrust and torque curves reflect primarily the effect of the wake-program correction factors (fig. 9).

Acoustics.- The acoustic pressure signatures of figure 10 were produced by utilizing aerodynamic data, such as those given in figure 7, with the linear acoustics program. It is seen that all the noise components are strong functions of blade tip speed and that the dominant noise mechanism is due to blade thickness. At a tip Mach number of 0.80, the skin-friction noise is greater than the loading noise while at the higher tip Mach numbers the opposite is true. The waveforms of these two noise components are such that they vary in opposite directions tending to cancel one another. Compared to thickness noise, skin-friction noise is negligible as shown in these figures.

The relative insignificance of skin-friction noise is also shown in figure 11. This figure shows the calculated overall sound pressure levels of thickness, loading and skin friction noise as a function of tip Mach number. For comparison, the overall sound pressure level of the combined effects of these three mechanisms is also shown in this figure. Only thickness noise is seen to be significant in the rotor plane; loading noise becomes relatively large out of the plane; skin-friction noise is small in all cases.

The calculated and measured overall acoustic pressure signatures are shown in figure 12. It is seen that the inclusion of the loading and the skin-friction noise in the overall acoustic pressure signatures has only changed slightly the peaks in the signature due to the thickness noise alone. This has only resulted in slightly better agreement with the experimental waveform shapes than those reported in reference 4. The theoretical and measured acoustic spectra for tip Mach number 0.80 through 0.962 are presented in figure 13. Thus the calculations of this report uphold the conclusions of

Boxwell et al (ref. 4) which were based on theoretical calculations of thickness noise alone. Basically, these conclusions refer to the width of the main pulse and the level of the pulse, described by its peaks, of the acoustic pressure signatures. These are:

i) linear acoustic theory predicts the pulse width and shape correctly at lowest tip speed (M_t = .8) but underpredicts the width and fails to account for the steepening of the pulse at near sonic speed (M_t = 0.962).

ii) linear acoustic theory predicts correctly the main peak of the pressure signature at near sonic speed but underpredicts (by a factor of almost 1/2) the main peak at M_t = 0.8. As the acoustic spectra show (fig. 13) the spectrum levels are also mostly underpredicted over the whole range of tip speeds.

Our experience with high-speed propeller and helicopter rotor noise calculations substantiates the above conclusions. However, the degree of the underprediction in the levels of the harmonics for the cases reported here is unexpectedly high. The reason for this is unknown to us. Better agreement between linear acoustic theory and experiment is reported by Farassat and Brown (ref. 15), Johnson and Lee (ref. 16), Mixson et al (ref. 17) and Woan and Gregorek (ref. 18).

Nonlinear flow effects around the blades have been suggested by Hanson and Fink (ref. 2) and by Yu, Caradonna and Schmitz (ref. 3) as the cause of the discrepancies between theoretical linear acoustic predictions and measured data. The present results indicate that this suggestion is correct. In the next section some remarks concerning the application of the acoustic analogy to include the nonlinearities are presented. A possible alternative to this method is also proposed.

REMARKS ON THE APPLICATION OF ACOUSTIC ANALOGY IN THE STUDY OF NONLINEAR EFFECTS

Although the concept of acoustic analogy is mathematically sound and there is little doubt that one can calculate the acoustic pressure provided that all sources and source strengths are known, one is forced to approximate the source strengths in practical situations. The question of how well one must approximate the source strengths to be able to calculate the level and the basic features of the acoustic pressure signature has not yet been answered. It is a well-known fact that what is called the solution of the FW-H equation in the acoustic literature is actually an integral equation. The very unknown that one is solving for also appears in the integrand of the solution. The appeal of the acoustic analogy so far has been that relatively little information (blade geometry and load) is required to calculate the noise of a rotating blade throughout the space around it. Much more information is now needed (the flow field around the blade) to include nonlinear effects using quadrupole sources.

Both Hanson and Fink (ref. 2) and Yu et al (ref. 3) start with equivalent forms of the solution of the FW-H equation involving the quadrupole source term. Hanson and Fink preferred to work in the frequency domain. Hanson and Fink's expression for quadrupole noise takes into consideration the discontinuities produced by shock waves on the blades, but in their numerical work, two-dimension flow around each blade strip was used to calculate the quadrupole source strength. The two-dimensional flow assumption may be reasonable only near the blade surface and away from the blade tip region. Near blade tips the deviation between two- and three-dimensional flow calculation is significant.

This fact was recognized by Yu et al who found that quadrupole noise calculations based on a two-dimensional flow model overpredicted the measured data. However, when a three-dimensional flow model was used and only the quadrupole sources up to the sonic surface in the rotating frame (blade-fixed) were considered, the calculations underpredicted the measured data. The restriction of sources to extend up to the sonic surface is itself an approximation which is forced on the authors because of the singularity in their acoustic formulation. This singularity is artificial and appears because of the use of blade-fixed coordinates. The discontinuities in flow parameters due to shock waves which may contribute to the radiated noise (refs. 19 and 20) were neglected in the approach of Yu et al.

The above discussion is intended to point out that there are many approximations that one is forced to introduce to include nonlinear effects in the acoustic calculation. Although all these approximations appear rational and logical, only extensive numerical calculations and comparison with experimental data can justify their appropriateness. It is, however, easy to show by the following nonlinear model problem that the flow field around the blades should perhaps be known to a high degree of accuracy.

The model problem which is studied here is that of a pulsating sphere in a medium with no mean flow. The sphere is assumed to pulsate with a surface velocity of the order of the normal velocities found on most parts of a conventional high-speed rotating blade. The pulsation frequency is assumed high enough so that the boundary conditions of the problem may be specified on the mean position of the sphere surface. (The effect of this assumption will be discussed later.) This problem can be solved by several perturbation techniques. Linear (first order) approximation does not exhibit the wave

steepening phenomenon and the formation of spherical shock waves separated by a wavelength of oscillation (ref. 21, chap. 9). The question is whether one may approximate the quadrupole strength in the FW-H equation, based on the first order solution of the problem, which can be obtained quite easily, to study such nonlinear phenomena.

The small parameter ε of the problem will be taken as the maximum of the sphere surface Mach number. If each flow parameter A (e.g., p and ρ) is expanded as

$$A = A_0 + \varepsilon A'_1 + \varepsilon^2 A'_2 + \ldots \equiv A_0 + A_1 + A_2 + \ldots \tag{2}$$

then the Lighthill stress tensor will become, up to the second order,

$$T_{ij} = \rho_0 u_{1i} u_{1j} + \frac{\gamma-1}{2\rho_0} c_0^2 \rho_1^2 \delta_{ij} \tag{3}$$

where c_0 is the speed of sound in the medium without the presence of the disturbance (same as c in eq. (1)). In eq. (3), γ is the ratio of the specific heats of the medium, and u_{1i} is the first-order velocity of the fluid with respect to the undisturbed medium. The solution of this problem formulated by acoustic analogy may be obtained numerically to find the acoustic pressure $p'(\vec{x},t)$. One may have to assume $p_2 << p_1$ on the surface of sphere at this stage, which is again a reasonable assumption. This method will not be attempted here because the same result can be obtained by solving for the second-order velocity potential of the acoustic field around the sphere. Some of the details of the following discussion are presented in Appendix C.

The differential equation for the second order velocity potential ϕ_2 is

$$\frac{1}{c^2}\frac{\partial^2 \phi_2}{\partial t^2} - \nabla^2 \phi_2 = -\frac{1}{2\rho_0^2 c_0^2}\frac{\partial}{\partial t}\left[(\gamma-1)c_0^2 \rho_1^2 + 2\rho_0^2 u_1^2\right] \tag{4}$$

where $u_1^2 = u_{1i}u_{1i}$. This equation can be solved analytically. If the radius of sphere is a and it is pulsating with the surface velocity $v = \alpha\sqrt{a'^2+1}\ \exp[-i(\omega t+\theta)]$ where $a' = ka$, $k = \omega/c_0$ and $\theta = \tan^{-1}(1/a')$, then one can show that

$$\phi_2(r,t) = \frac{\alpha^2 a'^4}{2\omega r'}\,[I(r')+ C]\ \exp\ (2i\xi). \tag{5}$$

Here $r' = kr$, $\xi = r'-a'-\omega t$ and

$$I(r') = \frac{\gamma+1}{2}\ \ln r' - \frac{i}{r'} - \frac{\gamma+1}{4}\ \exp(-4ir')[Ci(4r') + i\ Si(4r')] \tag{6}$$

The symbols Ci and Si stand for the cosine and sine integral functions, respectively, and the complex constant C is given by

$$C = \frac{2ia'+1}{2ia'-1}\ I(a') - \frac{1}{2ia'-1}\{4 + i\,[\frac{1}{a'} + (\gamma+1)a'\ln a']\} \tag{7}$$

Had the boundary condition been used on the actual surface of the sphere instead of its mean position, the expansion of the boundary condition would result in a second-order normal velocity term. This would affect equation (7), which is a constant term. In this case all the preceeding conclusions regarding this problem will remain true.

It can be shown that

$$p'_2 = -\rho_0 \frac{\partial\phi_2}{\partial t} + \frac{1}{2\rho_0 c_0^2}(p_1^2 - \rho_0^2 c_0^2 u_1^2)$$

$$= -\rho_0 \frac{\partial\phi_2}{\partial t} + 0\ (\frac{1}{r^3}) \tag{8}$$

By differentiating equation (5), we can find that the dominant term is logarithmic:

$$p'_2(r,t) = \frac{i\rho_0(\gamma+1)\alpha^2 a'^4}{r'} \ln r' \exp(2i\xi) + O\left(\frac{1}{r'}\right) \qquad (9)$$

This means that beyond some distance from the sphere center, p'_2 will be larger than p'_1 obtained from the linearized solution. Also the frequency of the acoustic oscillation will be the 2ω instead of ω. Since $p' = p'_1 + p'_2 + O(\varepsilon^3)$, the solution obtained by using acoustic analogy behaves the same. But this is absurd; it signifies the fact that the perturbation solution is not valid far from the sphere and a singular perturbation problem exists. Thus a reasonable approximation (the description of quadrupole strength using first-order velocities) in the use of the acoustic analogy has lead to wrong conclusions concerning the wave behavior far from the sphere.

The nonlinear solution of this model problem can be obtained by the renormalization method described in Appendix C (choosing the primitive variable p'_2 to be renormalized (ref. 22)), the analytical method of characteristics (refs 22 and 23) or the nonlinearization method discussed by Whitman (ref. 21). All these methods give the same result: there is always both wave steepening and shock wave formation but at a slower rate than finite amplitude one-dimensional waves (ref. 21). This wave steepening is clearly observed in the data of Boxwell et al at the highest tip Mach number.

An example of the wave-steepening effect for the illustrative case of an oscillating sphere is shown in figures 14 and 15. As shown in Appendix C, the equations for the nonlinear first-order acoustic pressure and radial velocity of the fluid are given by

$$P_1 = -\frac{a'^2 M_S}{r'\sqrt{a'^2 + 1}} \sin(s)$$

$$M_1 = \frac{a'^2 M_S}{r'^2} \sqrt{\frac{r'^2 + 1}{a'^2 + 1}} \cos(s + \theta).$$

The sphere for the two figures has a radius of 0.1 m and the amplitude of the surface Mach number is taken as 0.1. It is oscillating at 2000 Hz. It is seen that on the sphere surface, the velocity and pressure are out of phase and are oscillating at 2000 Hz. However, at a distance of 1.2 m ($r' = 36.96$), where a shock is formed, the velocity and pressure are in phase, and the wave form contains many harmonics. This latter phenomenon is basically a nonlinear effect. (The increase in signal width shown in figure 12 is another significant result of nonlinear effects.)

The above discussion relates to the problem of rotating blade noise because current efforts to account for nonlinear effects are all based on the use of acoustic analogy by including the quadrupole sources in noise calculations (refs. 2 and 3). Acoustic analogy was developed by Lighthill for the problem of jet noise generation where the source region is confined to the turbulent volume of the jet which is generally small in comparison with the region where the noise is calculated. In the case of high speed rotors and propellers, the quadrupole source region is extended and often overlaps with the region where acoustic pressure is required (in fuselage noise calculation, for instance). Since accounting for nonlinear effects while using acoustic analogy may require a good knowledge of the near-field, as shown in the case of the above model, it seems plausible that a more direct approach to the

problem should be made. The aerodynamic and aeroacoustic problems can no longer be separated as commonly done in applying the acoustic analogy. It is very likely that the idealized problem of the nonlifting rotor with sharp leading edge can be attacked using a perturbation approach. The associated boundary-value problems should preferably be solved in closed form to observe the behavior of the acoustic waves. The perturbation problem is expected to be singular because of the infinite domain (ref. 23). From comparison of linear acoustic calculations with experimental data, it also appears that the asymptotic sequence involved in the perturbation is not the usual $\varepsilon, \varepsilon^2, \ldots$ sequence. If this sequence is $\psi_i(\varepsilon)$, $i = 1, 2, \ldots$, then because of the magnitude of the correction required to improve linearized results, it follows that $\psi_2(\varepsilon)$ is much larger order than ε^2.

CONCLUDING REMARKS

An analytical study has been conducted to evaluate the accuracy with which linear acoustic methods can model the acoustic characteristics of rotor blades operated with transonic tip speeds. Using full aerodynamic data as input, linear acoustic calculations are presented and compared with measured cases reported by Boxwell, Yu and Schmitz. Depending on the blade tip Mach number, linear acoustic theory is shown to underpredict the peaks, width or wave-steepening effects for the main pulse of the acoustic pressure signature. Also, the noise component due to skin friction was shown to be virtually negligible compared to thickness noise. For inplane acoustic calculations, the thickness source mechanism was shown to be more significant than the blade loading sources. These results uphold the conclusions of Boxwell, Yu and Schmitz concerning the importance of nonlinear effects.

Some of the approximations involved in the application of acoustic analogy using quadrupole sources are discussed. By means of a model nonlinear problem it was shown that even a reasonable approximation of the flow field around a pulsating sphere, that is, the use of quadrupole source strength based on first-order fluid velocity, can result in wrong conclusions about the nature of the acoustic field. The requirement of good knowledge of quadrupole source strength in the near field implies that the aerodynamic and aeroacoustic problems must not be separated for high-speed rotating blades. It is suggested that the perturbation approach be used to study the nonlinear flow effect for a related idealized problem.

APPENDIX A

ACOUSTIC COMPUTER PROGRAM

To properly implement equation (1), it is necessary to accurately describe the blade in three dimensions and to have a good description of the blade-surface aerodynamics. The following is a brief description of both the geometry used in the computer program and required inputs. The generation of inputs describing local aerodynamics is discussed in a subsequent section.

The blade surface is represented by a series of panels. A conventional rectangular division scheme may give a poor approximation near the leading edge; therefore, a curvilinear coordinate system was selected. For each blade, a rotating Cartesian frame (η - frame) was set up such that the η_2-axis lies spanwise along the pitch-change axis of the blade and the η_3-axis extends along the shaft axis. The origin of this frame is located at the rotor (or propeller) center. A new variable, Q, is introduced in the chordwise direction and is defined as a distance along the local mean chord, measured from the leading edge and divided by the local chord. In the case of a rectangular blade, the Q and η_1 axes are coincident. The coordinates (Q, η_2, η_3) specify the blade surface completely. The blade is segmented by constant-η_2 planes normal to the pitch-change axis and by constant Q curves on the blade. For the rotor in use, these elements of area are rectangles lying on a slightly curved surface.

The full set of required inputs includes details of the rotor configuration, local aerodynamics and test conditions. The geometric parameters include number of blades, blade radius and both the local values and local spanwise derivatives of the following:

a) blade pitch

b) blade chord

c) thickness ratio

d) leading-edge coordinates

For the midpoint of each segment (between the constant-η_2 planes and Q curves) for each surface, the following inputs are required:

a) thickness coordinate

b) derivative of thickness coordinate with respect to Q

c) aerodynamic pressure normal to local surface

d) skin friction value

The operating conditions for the program consist of rotor rotational speed, speed of sound and air density.

Acoustic results are obtained with the process described by the block flow chart of figure 1. To perform the required time differentiation on the blade integral in equation (4), the contributions of each panel are summed for a given observer time, t. The process is then repeated for the observer time, $t + \Delta t$. Differentiation is then done numerically. Note that equation (4) is written for an observer fixed with respect to the medium. (To perform the differentiation with a moving observer, the observer position is frozen at the observer time t for the calculation at observer time $t + \Delta t$.) After all the calculations have been performed, the acoustic pressure signature is Fourier analyzed to give an acoustic-pressure spectrum in blade harmonics. Also, values of thrust and power are calculated based on integration on the blade-surface pressure and shear values.

APPENDIX B

AERODYNAMICS COMPUTER PROGRAMS

Hovering Rotor Program

The prescribed wake analysis discussed in references 6, 7, and 8 was employed to predict blade aerodynamics and rotor-wake characteristics. The first part of the program generates a wake geometry based on aerodynamic and configuration input. Two key wake parameters, functions of rotor geometry and thrust, determine the tip vortex geometry. A second part of the program determines the distributions of both the vortex-element circulation and induced velocity for the rotor-and-wake model. Each blade is represented by a lifting-line segment; the wake is modeled with a lattice of vortex filaments that trail as a complex surface behind each blade. Strong filaments at the tip roll up into a tip vortex representation. Interactive calculations determine a compatible pattern of circulation values and detailed geometry for each filament of both the wake and rotor elements. The third part of the program uses strip-theory aerodynamics and airfoil-table data to compute performance parameters.

The program of this study differs from that of reference 6 in two respects. New programing incorporated tip-relief effects on lift and drag from reference 24. Also, the program logic was modified to remove iterations of blade pitch to achieve desired thrust coefficients. Instead, since blade pitch was fixed in the experiment, the thrust estimates governing wake geometry were adjusted iteratively to provide a match with the final computation of thrust coefficient.

Several strengths and weaknesses of the program are significant. Reference 7 offers the conclusions that wake geometry appears to be insensitive

Pages 23 – 24
Are Missing in Document
Please See Original

APPENDIX C

NONLINEAR FLOW EFFECT FOR A PULSATING SPHERE

This problem was treated by Whitham as an example of a nonlinearization technique (ref. 20). The basic nonlinear phenomena associated with this problem are therefore known. It was mentioned in the main text of this paper that this problem was used to test the acoustic analogy using input data from linear theory. Here some of the mathematical details of this problem will be presented.

Using an expansion of the type in equation (2) for the velocity potential ϕ, the first-order term can be shown to be

$$\phi_1(r,t) = \frac{f(r - a - c_0 t)}{r} \tag{C-1}$$

The function f is determined by specifying the velocity on the sphere. The second-order velocity potential is given by equation (4). Using complex notation and thus simplifying manipulations greatly, the sphere surface velocity is taken as

$$v = \alpha\sqrt{a'^2 + 1} \quad \exp\,[-i(\omega t + \theta)] \tag{C-2}$$

where α is real.

This results in the following form of ϕ_1:

$$\phi_1(r, t) = \alpha\, a^2 \, \frac{\exp\,(i\xi)}{r} \tag{C-3}$$

In what follows, only the real parts of complex quantities have physical meaning.

Equation (3) for ϕ_2 becomes

$$\frac{1}{c_0^2}\,\frac{\partial^2(r\phi_2)}{\partial t^2} - \frac{\partial^2(r\phi_2)}{\partial r^2} = \frac{\beta}{r^3}\left\{[2 - (\gamma+1)\,k^2r^2]\,i + 4kr\right\}\exp(2i\xi) \qquad \text{(C-4)}$$

where $\beta = \alpha^2 a^4 \omega/(2c_0^2)$. The boundary conditions on this equation are:

(i) $\dfrac{\partial\phi_2}{\partial r}(a, t) = 0$

(ii) $\phi_2 \to 0$ as $r \to \infty$

(iii) ϕ_2 satisfies the outgoing wave condition.

Assuming a solution of the following type for equation (C-4):

$$r\phi_2(r,t) = \beta\, B(r) \exp(2i\xi) \qquad \text{(C-5)}$$

the equation for finding $B(r)$ becomes

$$B'' + 4ik\,B' = -\frac{[2 - (\gamma+1)\,k^2r^2]i + 4kr}{r^3} \qquad \text{(C-6)}$$

The homogeneous solution of equation (C-6) which will result in an outgoing wave solution of equation (C-4), is a constant. A particular integral of equation (C-6) is easily obtained by integrating both sides of this equation once and then finding an integrating factor for the left side of the resulting equation. After applying the boundary conditions, equation (5) is obtained.

It is seen from equation (9) that the perturbation method breaks down far from the sphere center. To obtain the first-order solution valid in the far-field, the renormalization technique will be used. It is much simpler here to apply the method suggested by Pritulo (ref. 23). It is seen here that ξ

in equation (C-5) actually is the outgoing characteristic variable. A new variable s is introduced as follows:

$$\xi = s + \alpha S_1 (s, r') + \ldots\ldots$$

$$\xi (s, a') = s \tag{C-7}$$

This is substituted in p'_2 and the resulting expression is expanded as a power series in α. To get rid of the secular term involving $\ln r'$ in p'_2, we should have

$$c_0 S_1 \cos(s) + \frac{1}{4} (\gamma + 1)\, a'^2 \ln \left(\frac{r'}{a'}\right) \sin (2s) = 0 \tag{C-8}$$

This will give

$$S_1(r', s) = \frac{-(\gamma + 1)\, a'^2}{2\, c_0} \ln\left(\frac{r'}{a}\right) \sin(s) \tag{C-9}$$

The nonlinear first-order acoustic pressure and radial velocity of the fluid in nondimensional form are

$$P_1 = - \frac{a'^2 M_s}{r' \sqrt{a'^2 + 1}} \sin(s) \tag{C-10}$$

$$M_1 = \frac{a'^2 M_s}{r'^2} \sqrt{\frac{r'^2 + 1}{a'^2 + 1}} \cos(s + \theta) \tag{C-11}$$

where $P_1 = P_1'/(\rho_0 c_0^2)$, $M_1 = v_1/c_0$ and M_s is the amplitude of the surface Mach number of the sphere based on c_0. The phase angle θ is given by

$$\theta = -\tan^{-1} (1/r'). \tag{C-12}$$

The variable ξ is given by equation (C-7) and can also be written as follows

$$\xi = s - \frac{(\gamma + 1)\, a'^2\, M_s}{2\sqrt{a'^2 + 1}} \ln\left(\frac{r'}{a'}\right) \sin(s) \qquad \text{(C-13)}$$

All the above equations are valid up to the location where the first shock appears near the sphere surface.

REFERENCES

1. Ffowcs Williams, J. E. and Hawkings, D. L.: Sound Generation by Turbulence and Surfaces in Arbitrary Motion. Philosophical Transactions of the Royal Society of London, vol. 264A, 1969, pp. 321-342.

2. Hanson, D. B; and Fink, M. R.: The Importance of Quadrupole Sources in Prediction of Transonic Tip Speed Propeller Noise. Paper presented at Spring Meeting of the Institute of Acoustics, Cambridge University, England, Apr. 7, 1978.

3. Yu, Yung H.; Caradonna, Frank X.; and Schmitz, Fredric H.: The Influence of the Transonic Flow Field on High-Speed Helicopter Impulsive Noise. Paper no. 58, Fourth European Rotorcraft and Powered Lift Aircraft Forum. Sept. 1978, Stresa, Italy.

4. Boxwell, D. A.; Yu, Y. H.; and Schmitz, F. H.: Hovering Impulsive Noise - Some Measured and Calculated Results. Paper 15, Helicopter Acoustics, Part I, NASA CP 2052, 1978.

5. Farassat, F.: Theory of Noise Generation from Moving Blades with an Application to Helicopter Rotors. NASA TR R-451, 1975.

6. Landgrebe, A. J.: An Analytical and Experimental Investigation of Helicopter Rotor Hover Performance and Wake Geometry Characteristics, USAAMRDL TR 71-24, June 1971.

7. Landgrebe, Anton: The Wake Geometry of a Hovering Helicopter Rotor and Its Influence on Rotor Performance. J. American Helicopter Society, vol. 17, no. 4, Oct. 1972, pp. 3-15.

8. Langrebe, A. J.; Moffit, Robert C.; and Clark, David R.: Aerodynamic Technology for Advanced Rotorcraft - Part I. J. American Helicopter Society, vol. 22, no. 2, April 1977, pp. 21-27.

9. Bauer, Frances; Garabedian, Paul; Korn, David; and Jameson, Antony: Supercritical Wing Sections II. Lecture Notes in Economics and Mathematical Systems, vol. 108, Springer-Verlag (New York), 1975.

10. Bauer, Frances; Garabedian, Paul; and Korn, David: Supercritical Wing Sections III. Lecture Notes in Economics and Mathematical Systems, vol. 150, Springer-Verlag (New York), 1977.

11. Garabedian, P. R.: Transonic Flow Theory of Airfoils and Wings. Advances in Engineering Science. vol. 4. NASA CP-2001, 1976, pp. 1349-1358.

12. Farassat, F.; Morris, C. E. K., Jr.; and Nystrom, P. A.: A Comparison of Linear Acoustic Theory with Experimental Noise Data for a Small-Scale Hovering Rotor. AIAA 5th Aeroacoustics Conf. Paper No. 79-0608, March 1979.

13. Stevens, W. A.; Goradia, S. H.; and Braden, J. A.: Mathematical Model for Two-Dimensional Multi-Component Airfoils in Viscous Flow. NASA CR-1843, 1971.

14. Noonan, Kevin W.; and Bingham, Gene J.: Two-Dimensional Aerodynamic Characteristics of Several Rotorcraft Airfoils at Mach Numbers from 0.35 to 0.90. NASA TM X-73990, 1977.

15. Farassat, F.; and Brown, T. J.: A New Capability for Predicting Helicopter Rotor and Propeller Noise Including the Effect of Forward Motion. NASA TM X-74037, 1977.

16. Johnson, W.; and Lee, A.: Comparison of Measured and Calculated Helicopter Rotor Impulsive Noise. NASA TM 78473, 1978.

17. Mixson, J. S.; Barton, C. K.; Pierson, A. G.; and Wilby, J. F.: Characteristics of Propeller Noise on an Aircraft Fuselage Related to Interior Noise Transmission. AIAA 5th Aeroacoustics Conference. Paper No. 79-0646, March 1979.

18. Woan, C. J.; and Gregorek, G. M.: The Exact Numerical Calculation of Propeller Noise. AIAA Paper No. 78-1122. Presented at 11th Fluid and Plasma Dynamics Conference, Seattle, WA., July 10-12, 1978.

19. Farassat, F.: The Acoustic Far-Field of Rigid Bodies in Arbitrary Motion. J. Sound and Vibration, vol. 32(3), 1974, pp. 387-405.

20. Kitaplioglu, C.; and George, A. R.: A Study of Far Field Sound Due to Unsteady Shocks on Rotors. AIAA Paper No. 77-1360, 1977.

21. Whitham, G. B.: Linear and Nonlinear Waves. John Wiley & Sons. 1974.

22. Nayfeh, A. H.; and Kluwick, A.: A Comparison of Three Perturbation Methods for Nonlinear Hyperbolic Waves. J. Sound and Vibration, vol. 48(2), 1976, pp. 293-299.

23. Nayfeh, A. H.: Perburbation Methods. John Wiley & Sons. 1973.

24. LeNard, John M.; and Boeheler, Gabriel D.: Inclusion of Tip Relief in the Prediction of Compressibility Effects on Helicopter Rotor Performance. USAAMRDL TR 73-71, Dec. 1973.

25. Smetana, Fredrick O.; Summey, Delbert C.; Smith, Neill S.; and Carden, Ronald K.: Light Aircraft Lift, Drag and Moment Prediction - A Review and Analysis. NASA CR-2523, May 1975.

26. Brune, G. W.; and Manke, J. W.: A Critical Evaluation of the Predictions of the NASA-Lockheed Multielment Airfoil Computer Program. NASA CR-145322, Mar. 1978.

TABLE I.- ROTOR GEOMETRY

Hub type	teetering
Radius	1.045 m
Chord	0.0762 m
Taper	1.1
Twist (root-to-tip)	-10.91°
Blade pitch (at tip)	1.5°
Airfoil	NACA 0012

TABLE II.- ACOUSTIC PROGRAM TEST CONDITIONS

M_t	c (m/sec)	Ω (rpm)	ρ_0 (kg/m^3)
.80	340.75	2491.	1.2333
.88	339.64	2732	1.2133
.90	339.70	2793	1.2144
.962	340.46	2994	1.2281

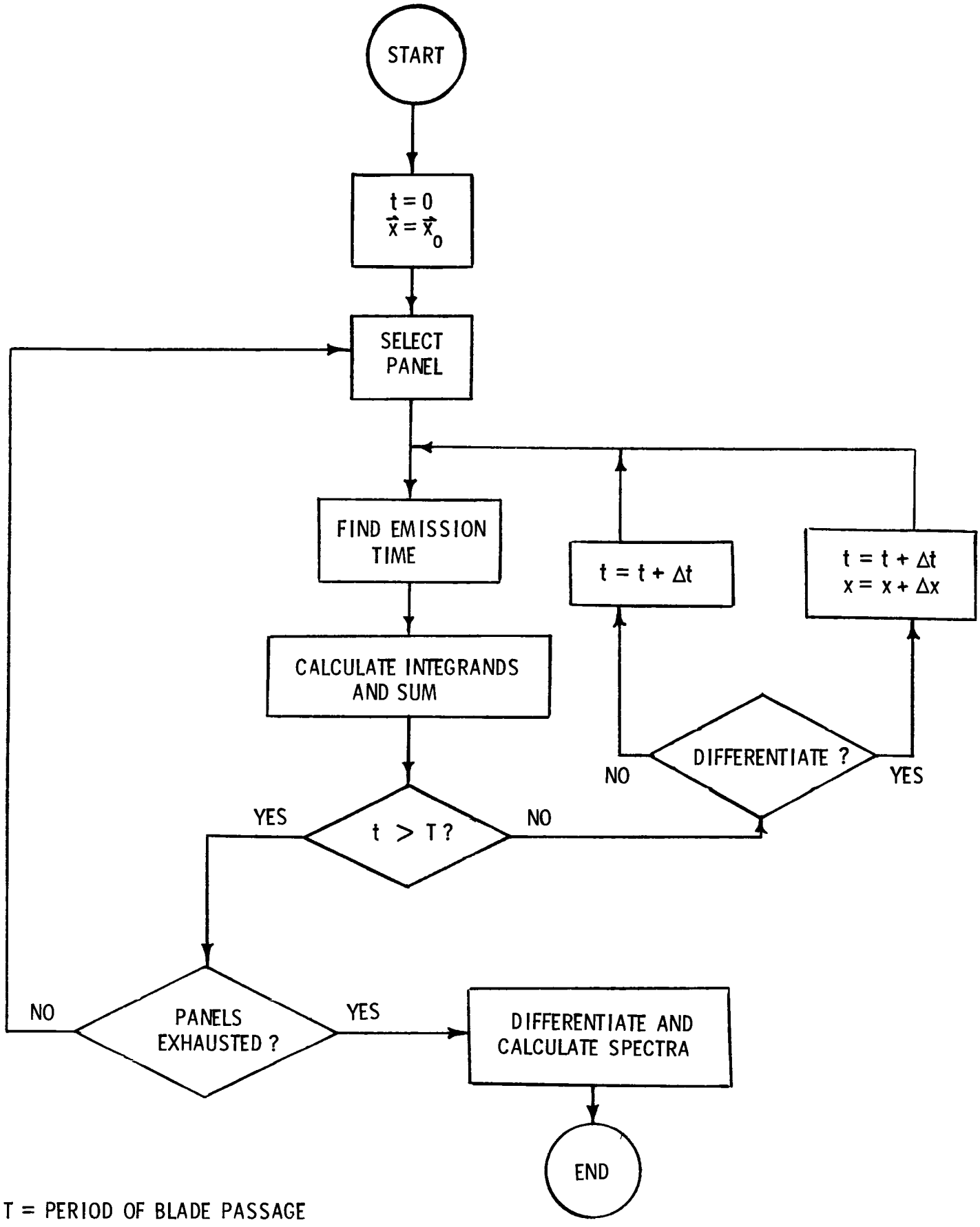

Figure 1. - Flow chart for the acoustic computer program.

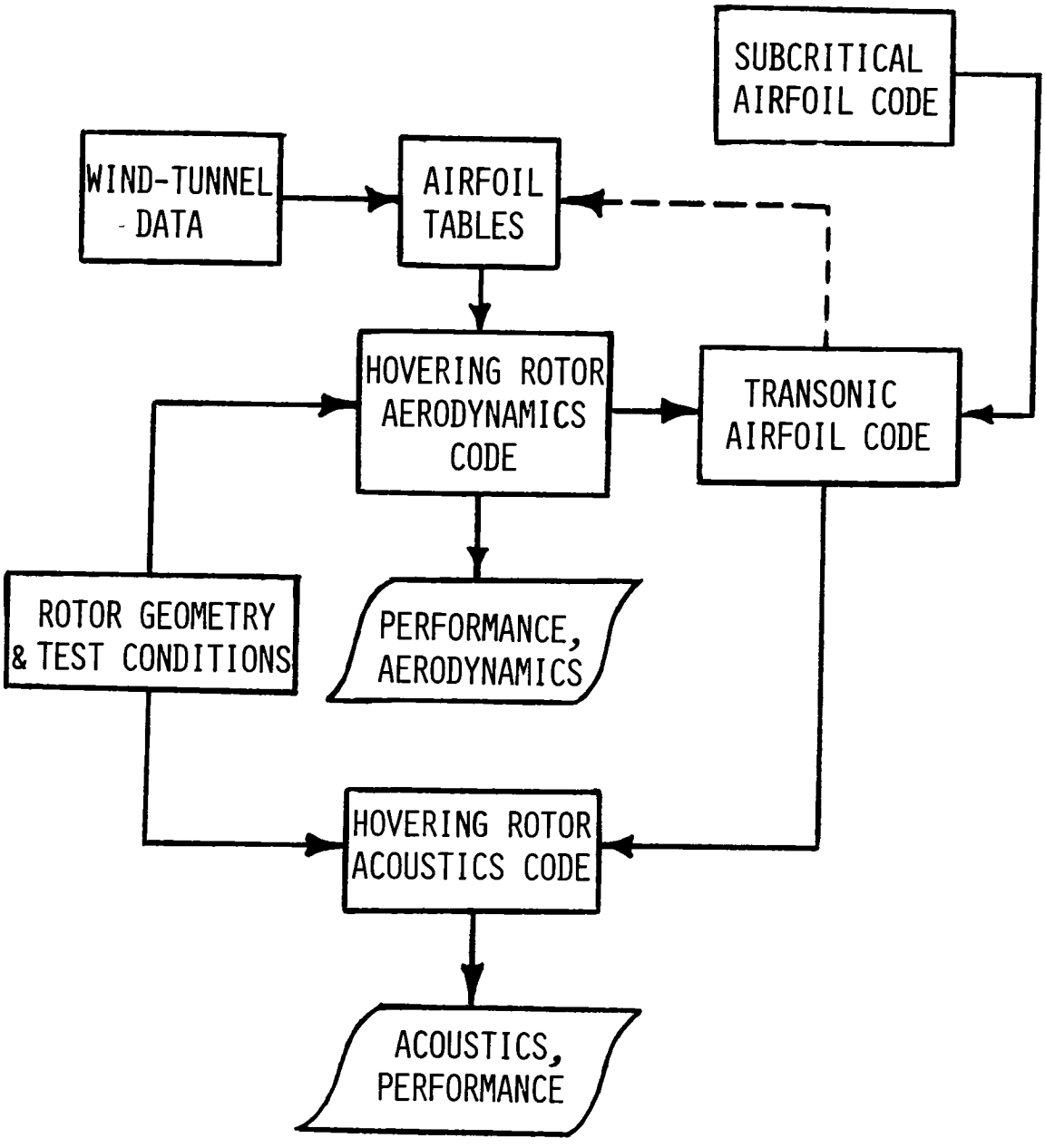

Figure 2. - Coupling of acoustic and aerodynamic methods.

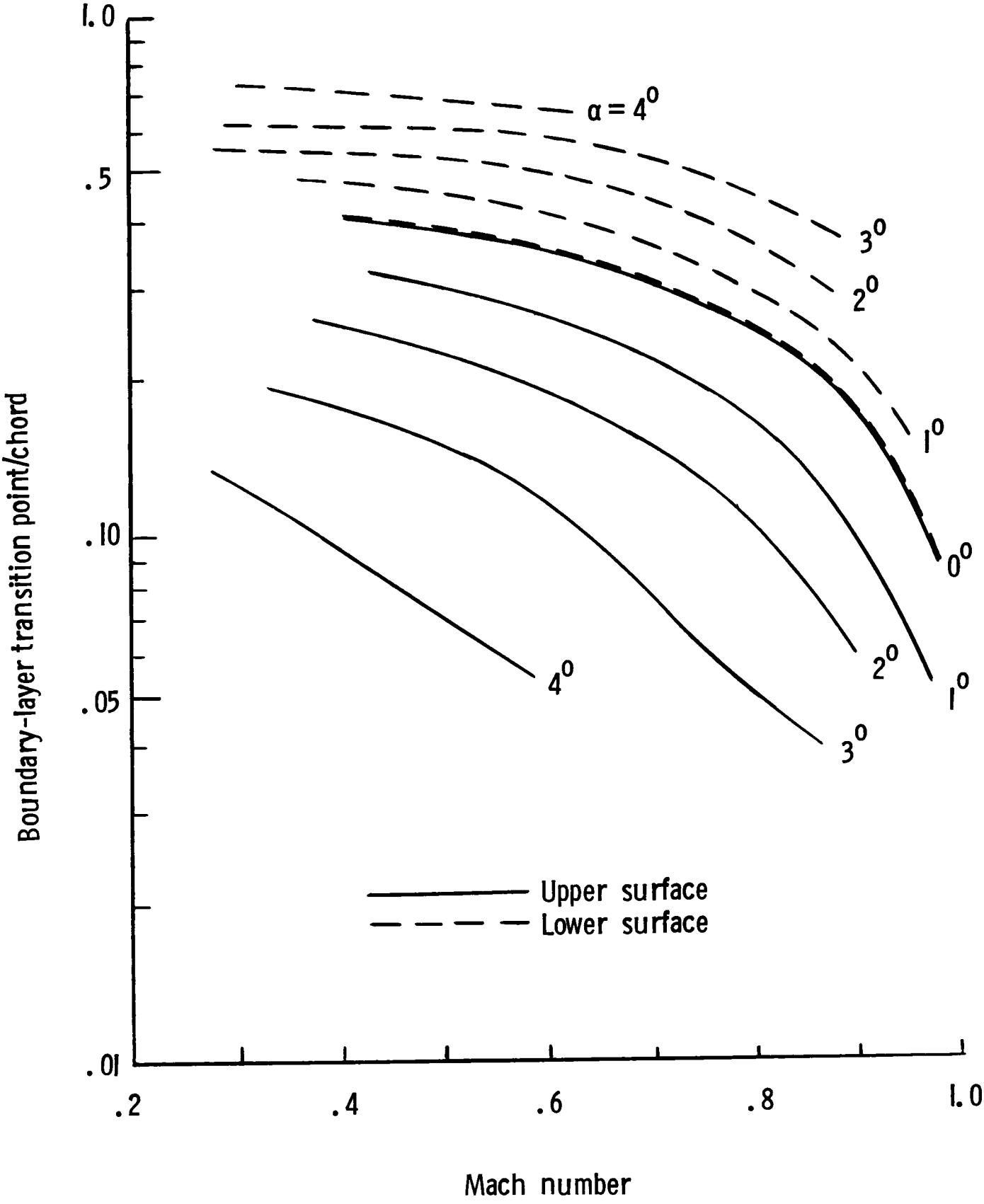

Figure 3. - Variation of predicted boundary-layer transition with Mach number of model blade section.

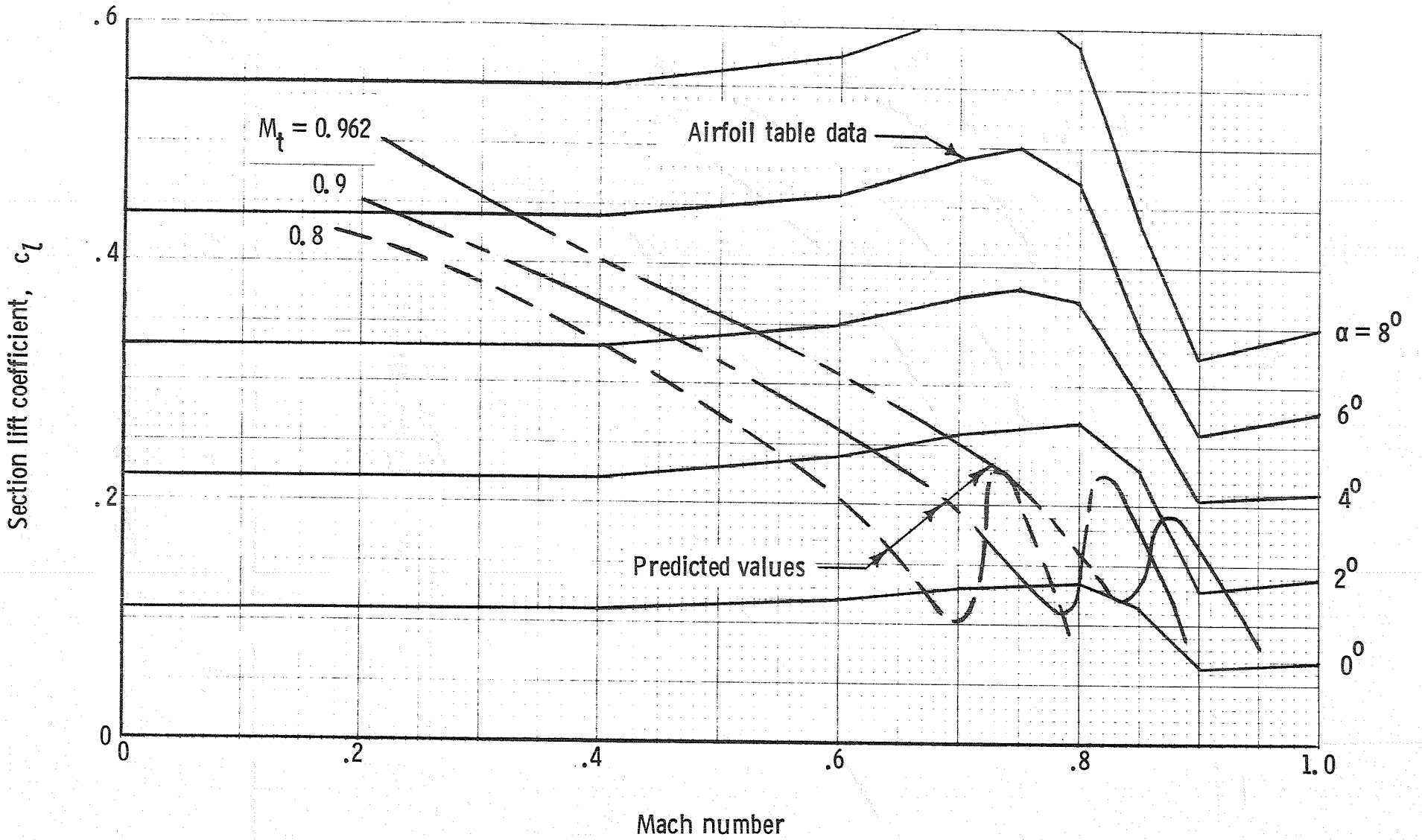

Figure 4. - Airfoil lift characteristics: data input and output for prescribed-wake rotor program.

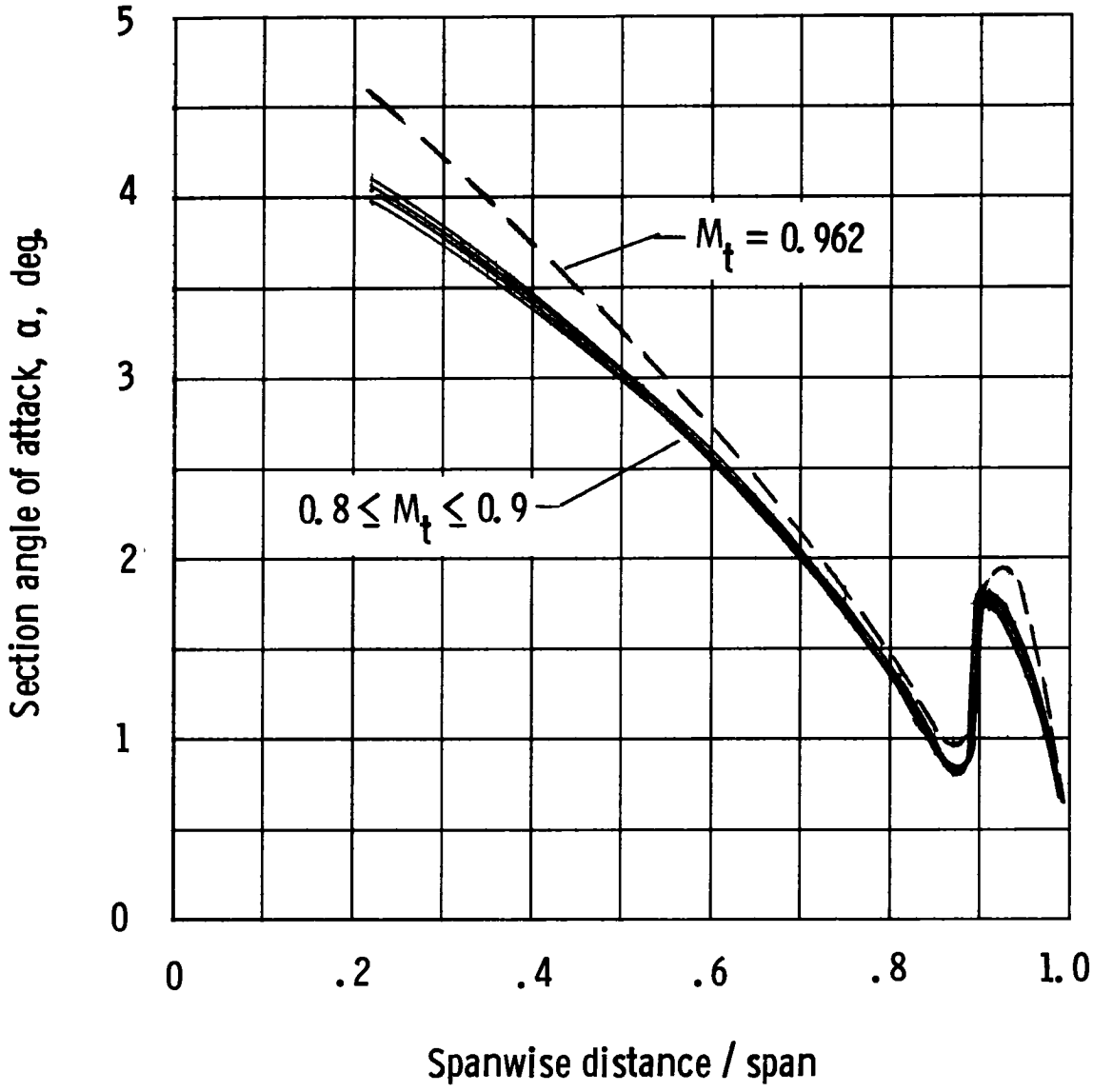

Figure 5. - Predicted spanwise distribution of effective angle of attack for hovering rotor.

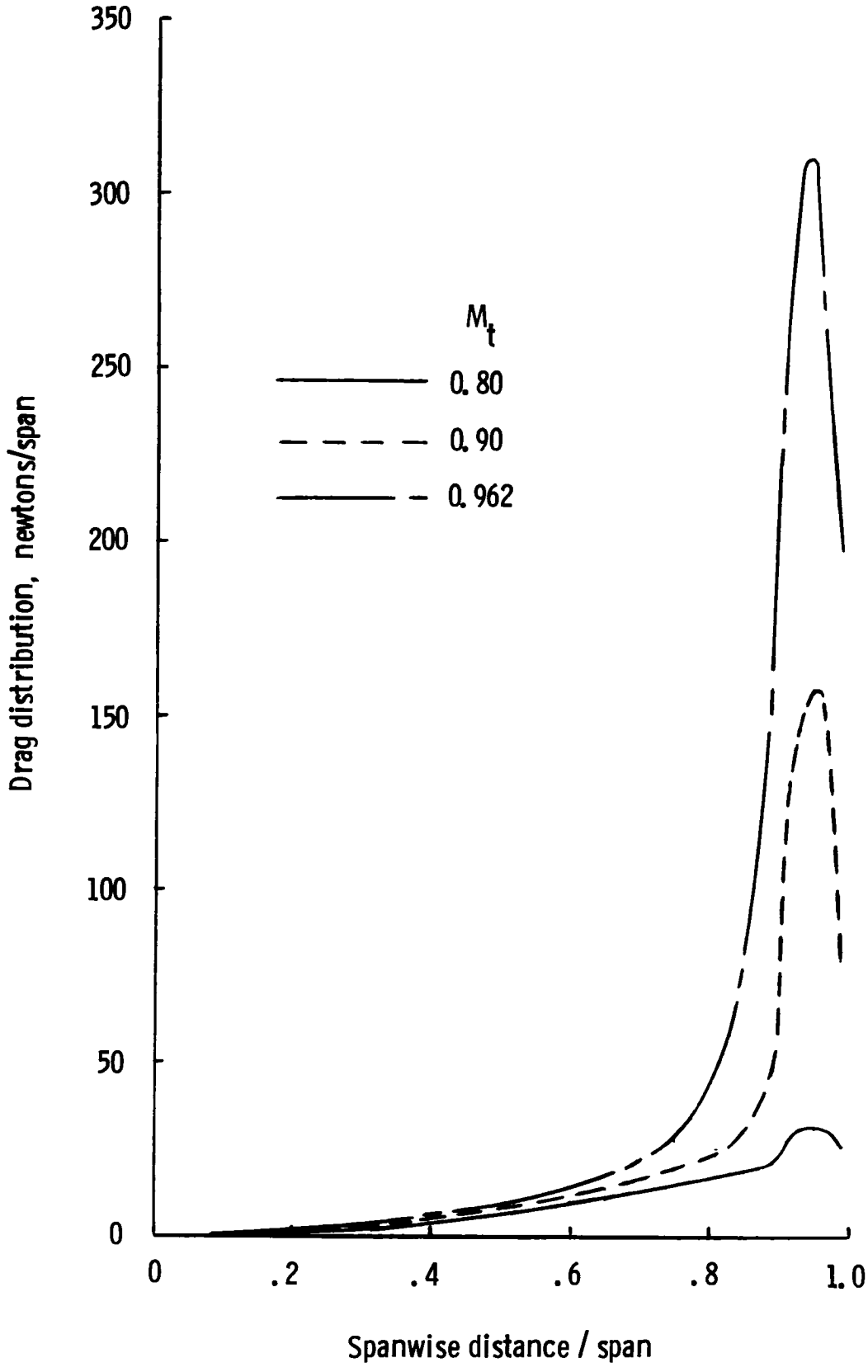

Figure 6. - Spanwise drag distribution predicted for hovering rotor by prescribed-wake program (ref 6).

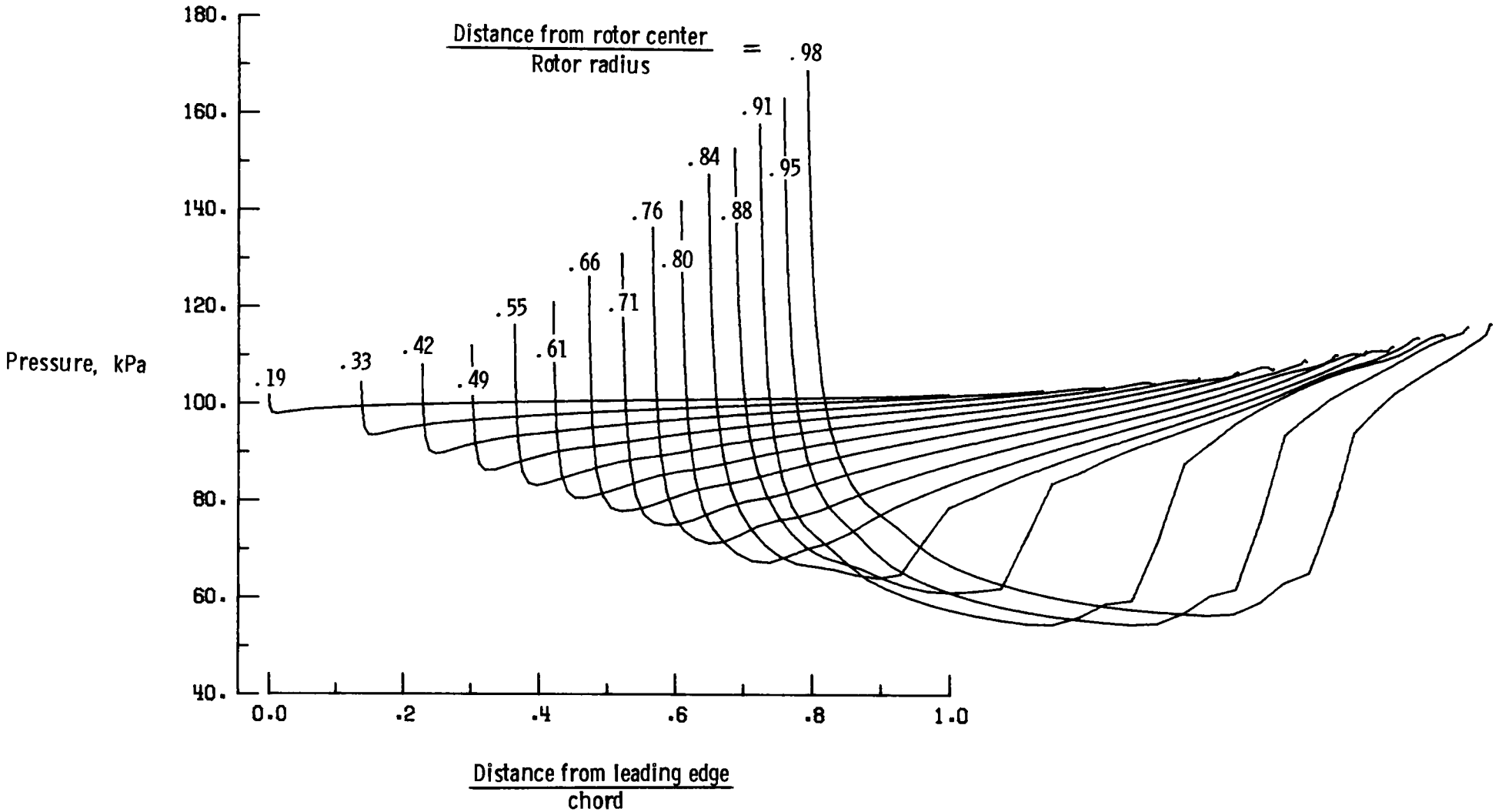

(a) Upper-surface pressure distribution

Figure 7. - Predicted distribution of surface pressure and tangential stress acting on a hovering rotor blade. $M_t = 0.9$.

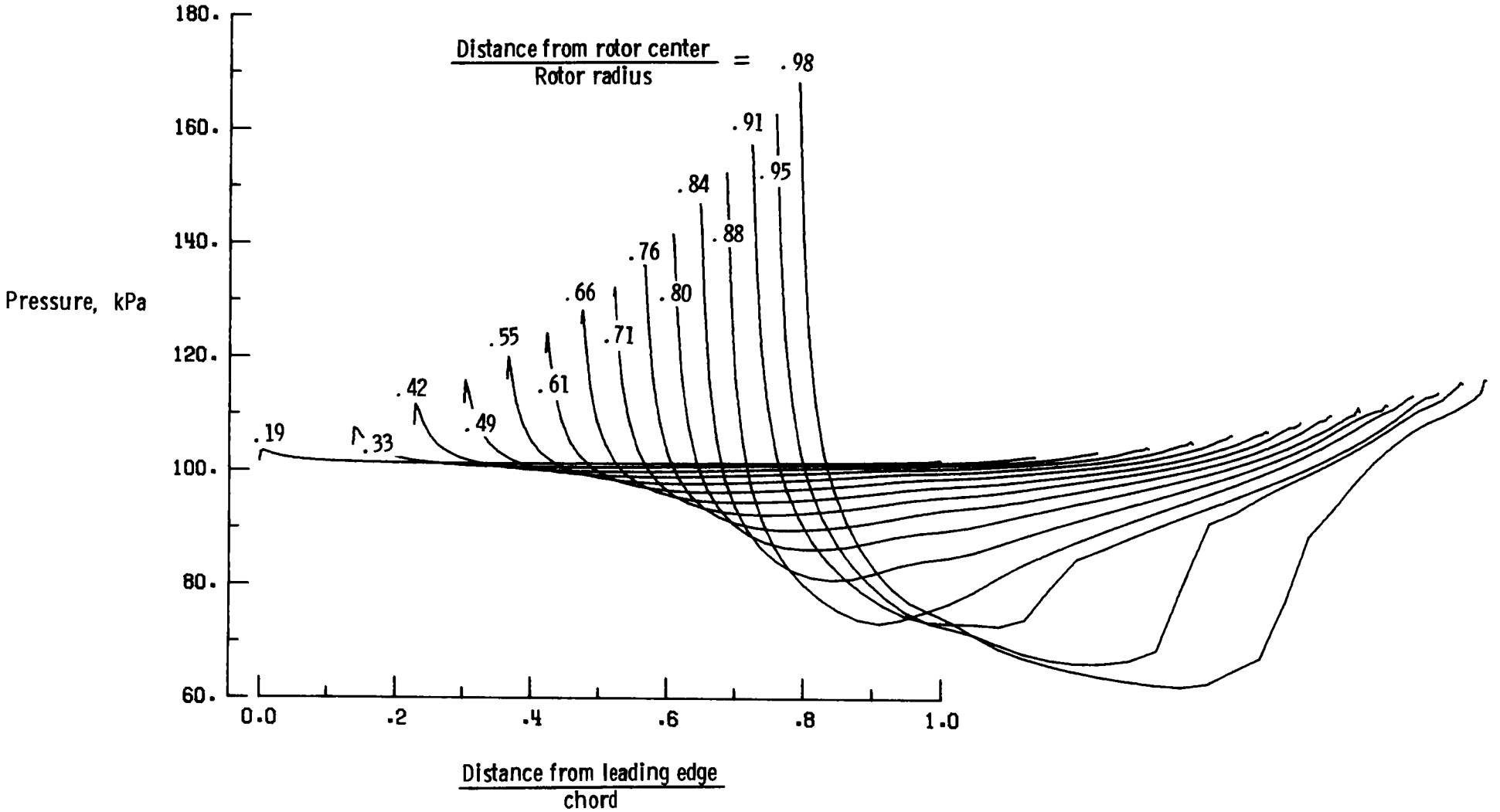

(b) Lower-surface pressure distribution

Figure 7. - Continued.

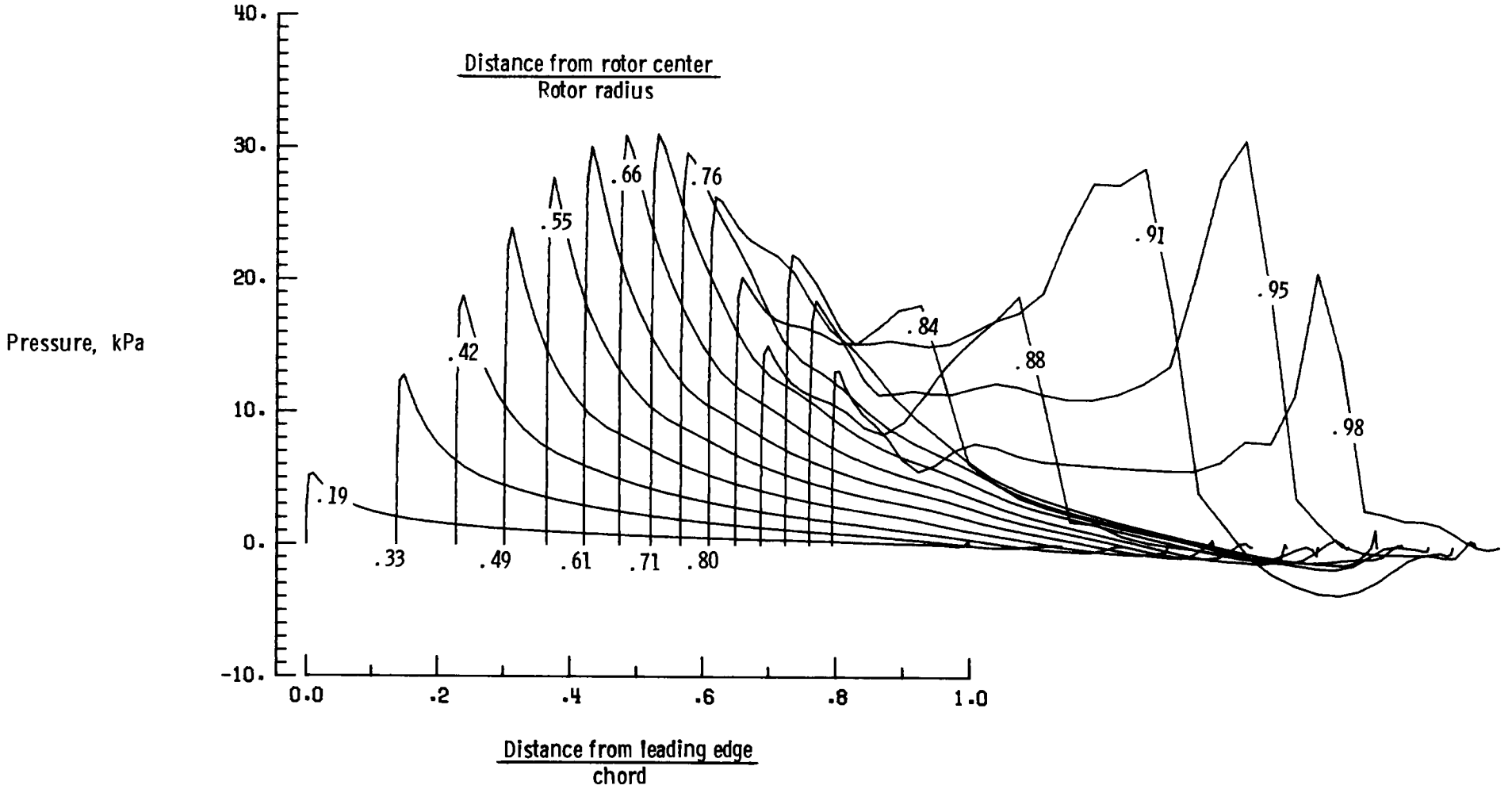

(c) Differential pressure distribution

Figure 7. - Continued.

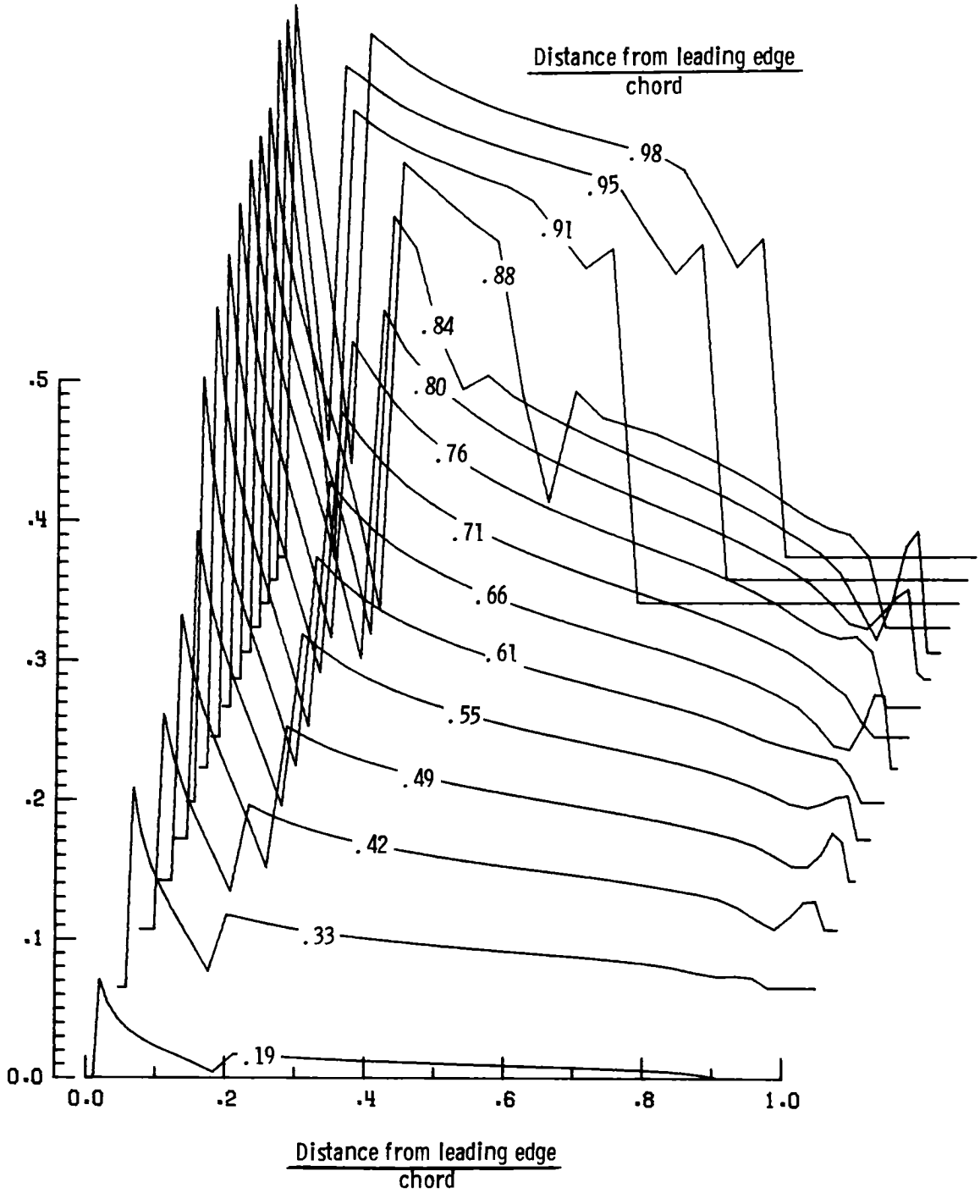

(d) Upper-surface shear stress distribution

Figure 7. - Continued.

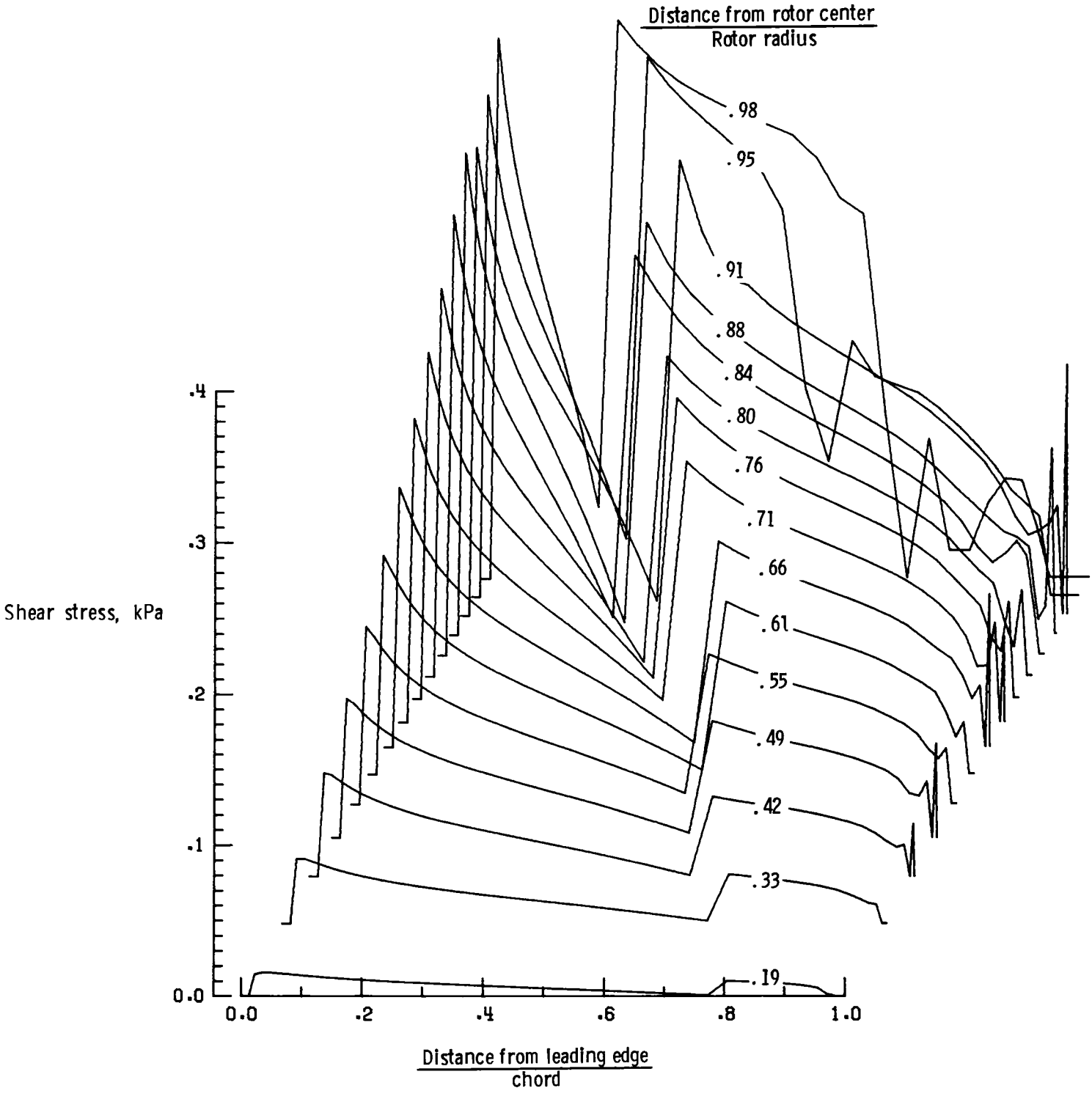

(e) Lower-surface shear stress distribution

Figure 7. - Concluded.

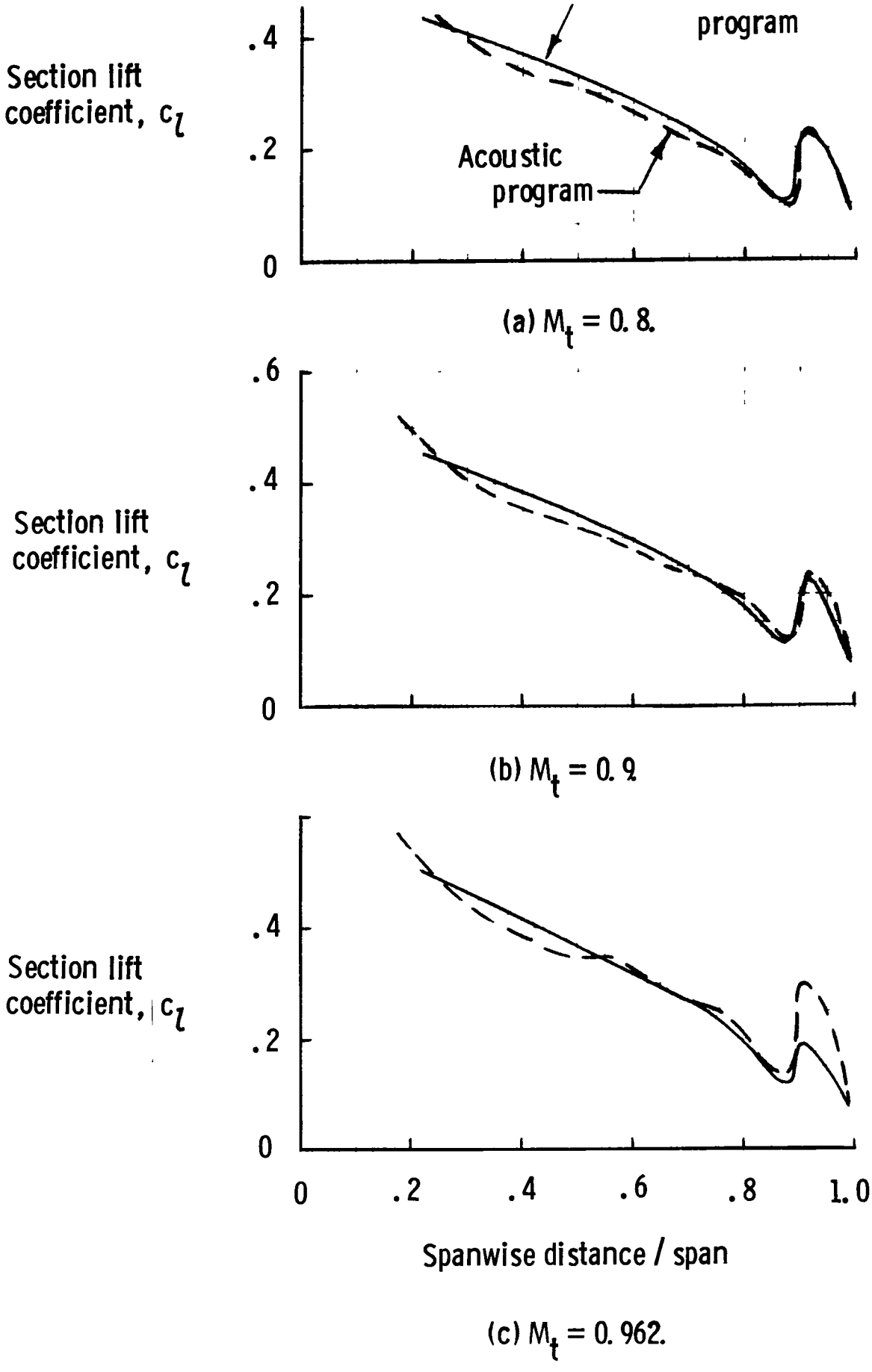

Figure 8. - Spanwise lift distributions calculated for hovering rotor with two methods.

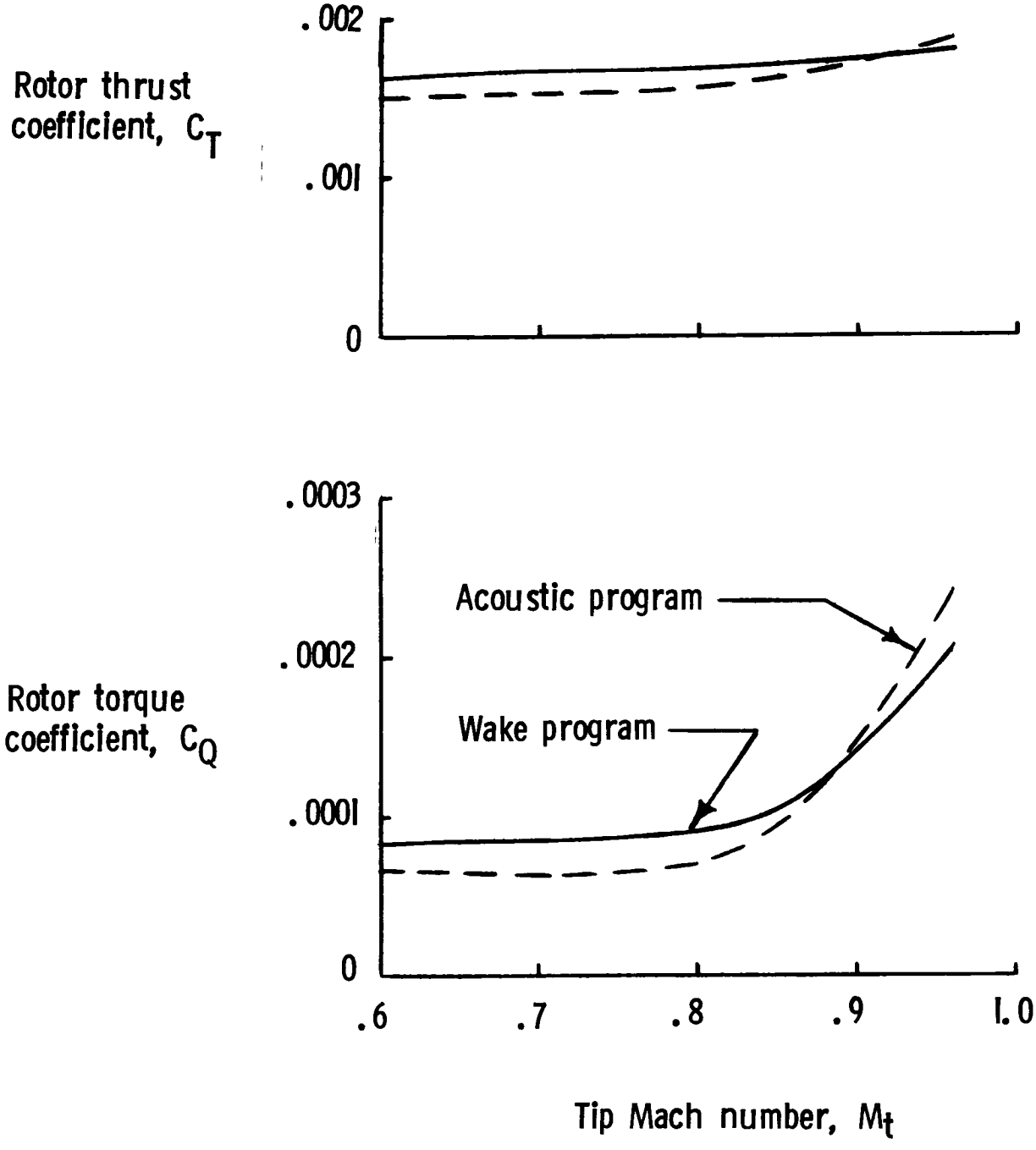

Figure 9. - Comparison of hovering rotor performance calculated with two methods.

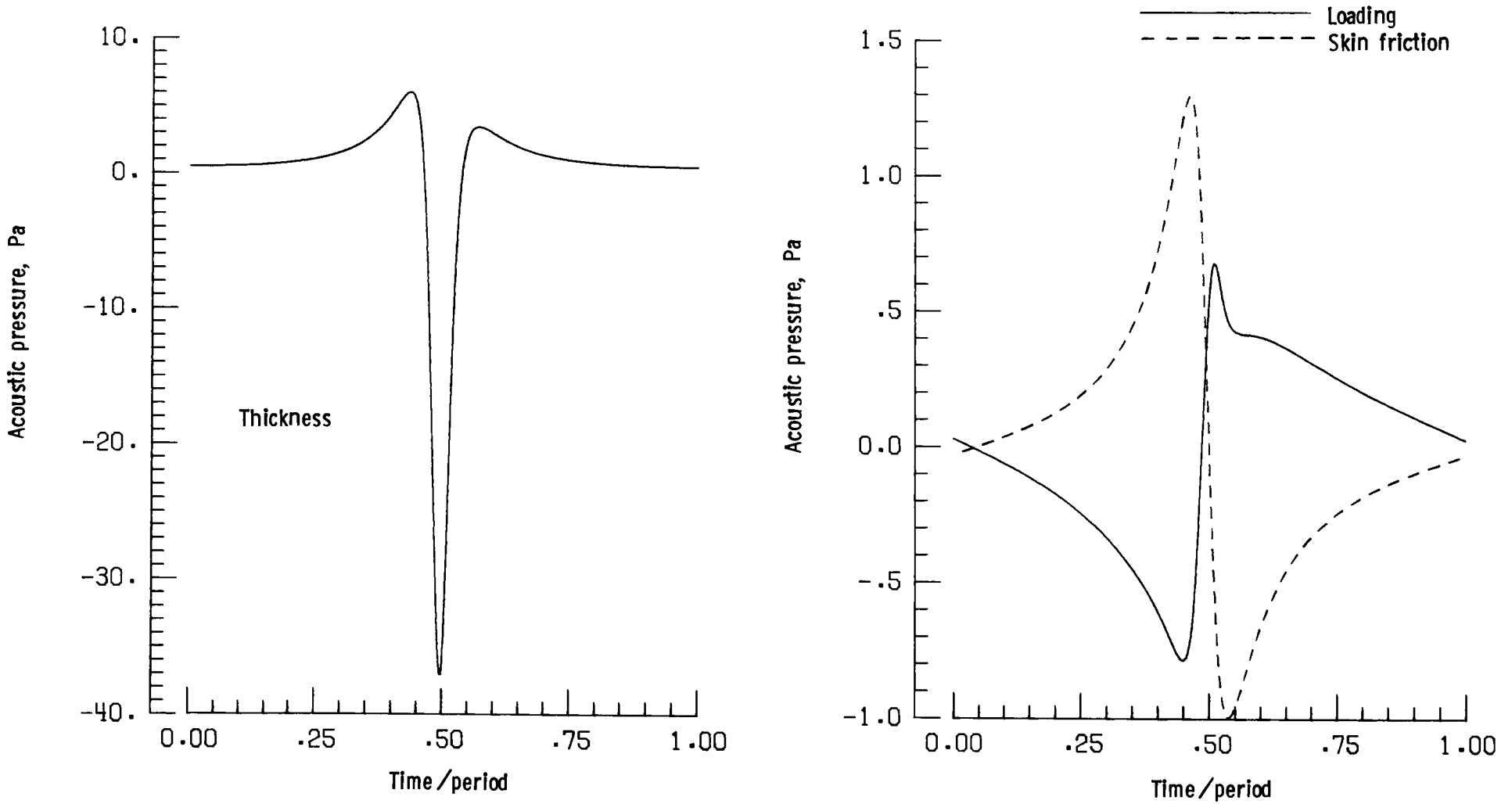

(a) M = 0.80

Figure 10. - Acoustic pressure sighatures of the inplane noise components for one period at 3 rotor radii from rotor center.

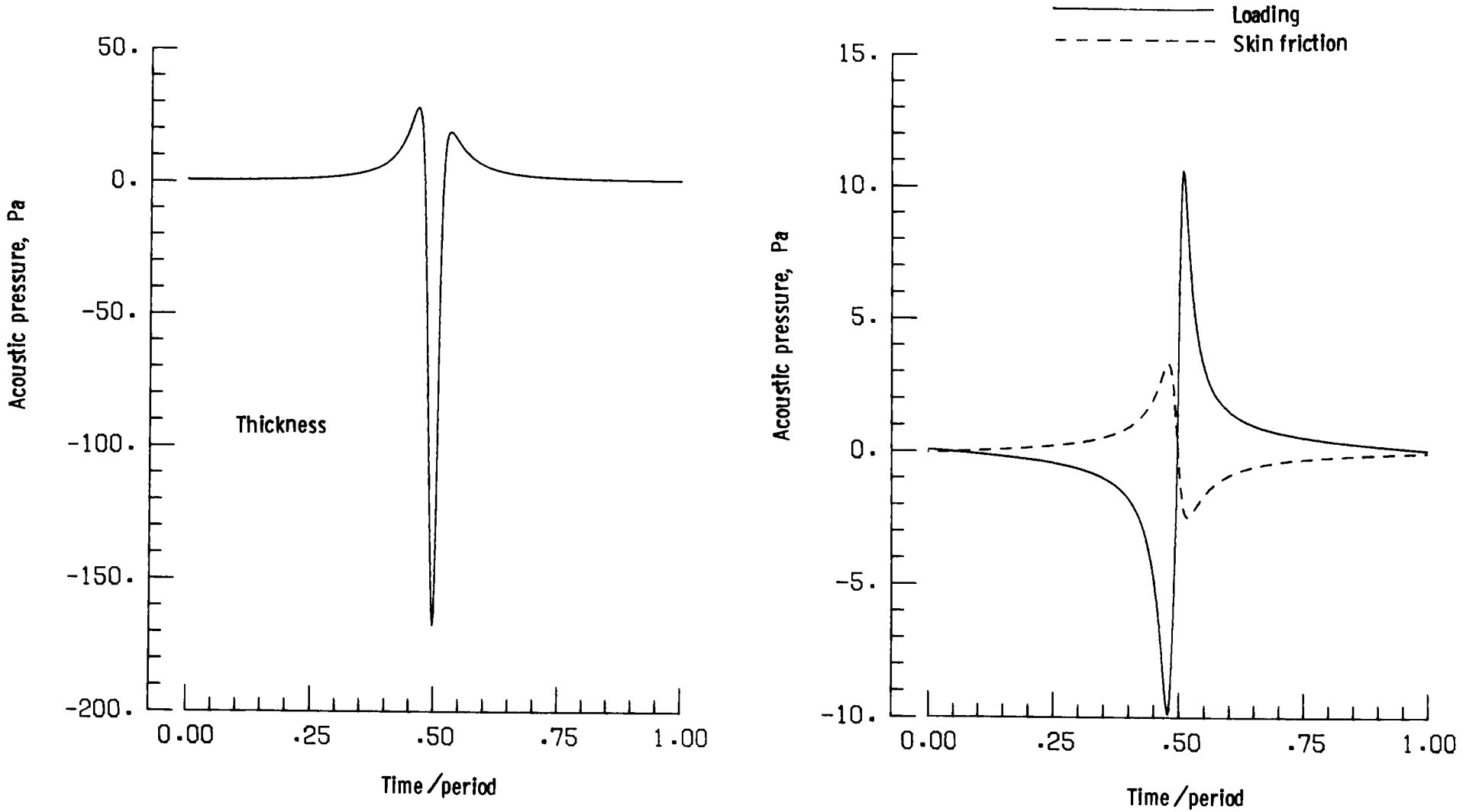

(b) $M_t = 0.88$

Figure 10. - Continued.

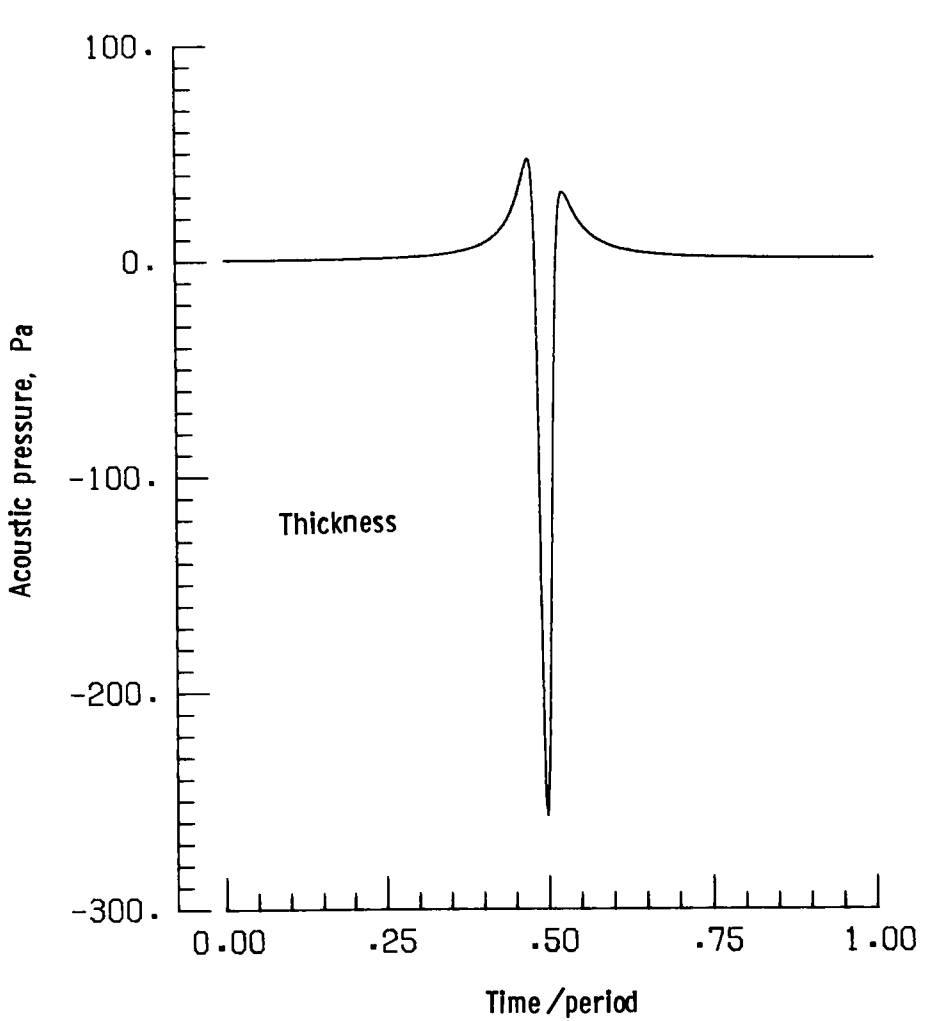

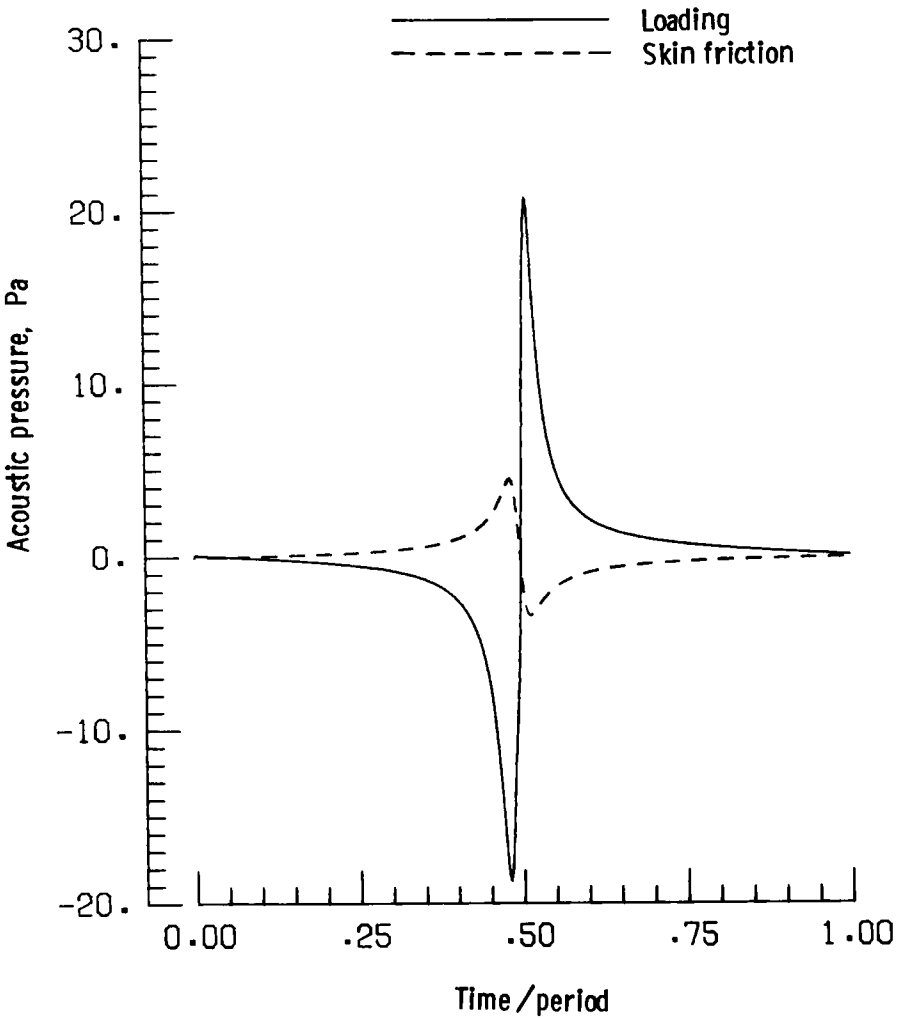

(c) $M_t = 0.90$

Figure 10. - Continued.

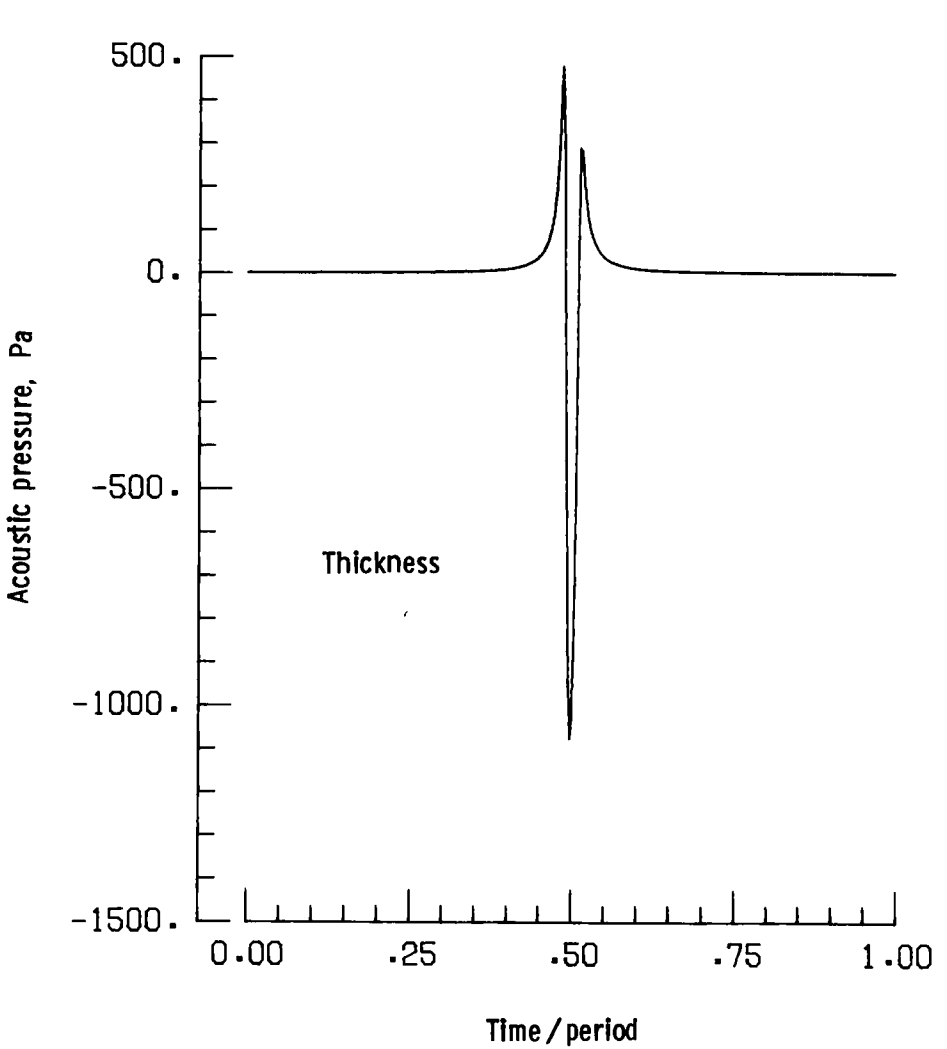

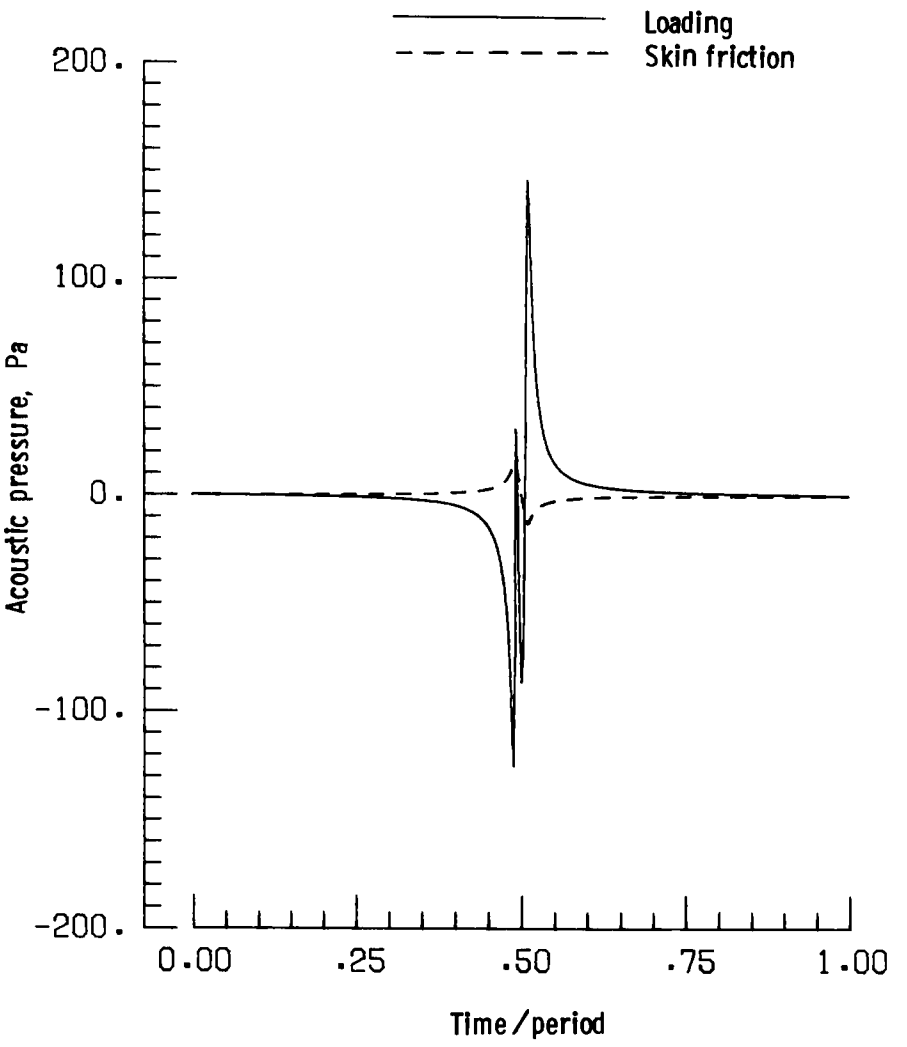

(d) $M_t = 0.962$

Figure 10. - Concluded.

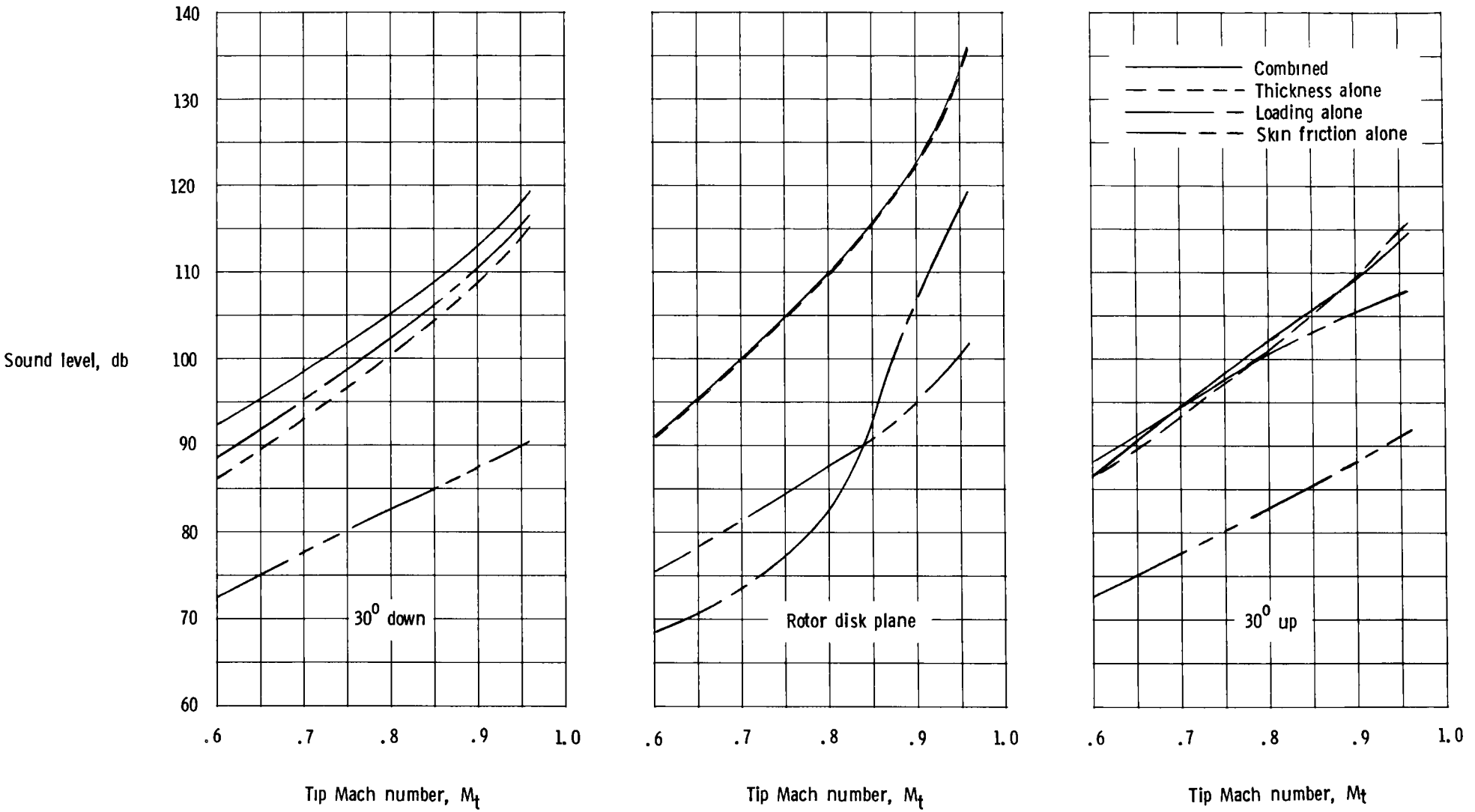

Figure 11. - Calculated overall sound pressure level for combined and separate component noise at 3 rotor radii from rotor center.

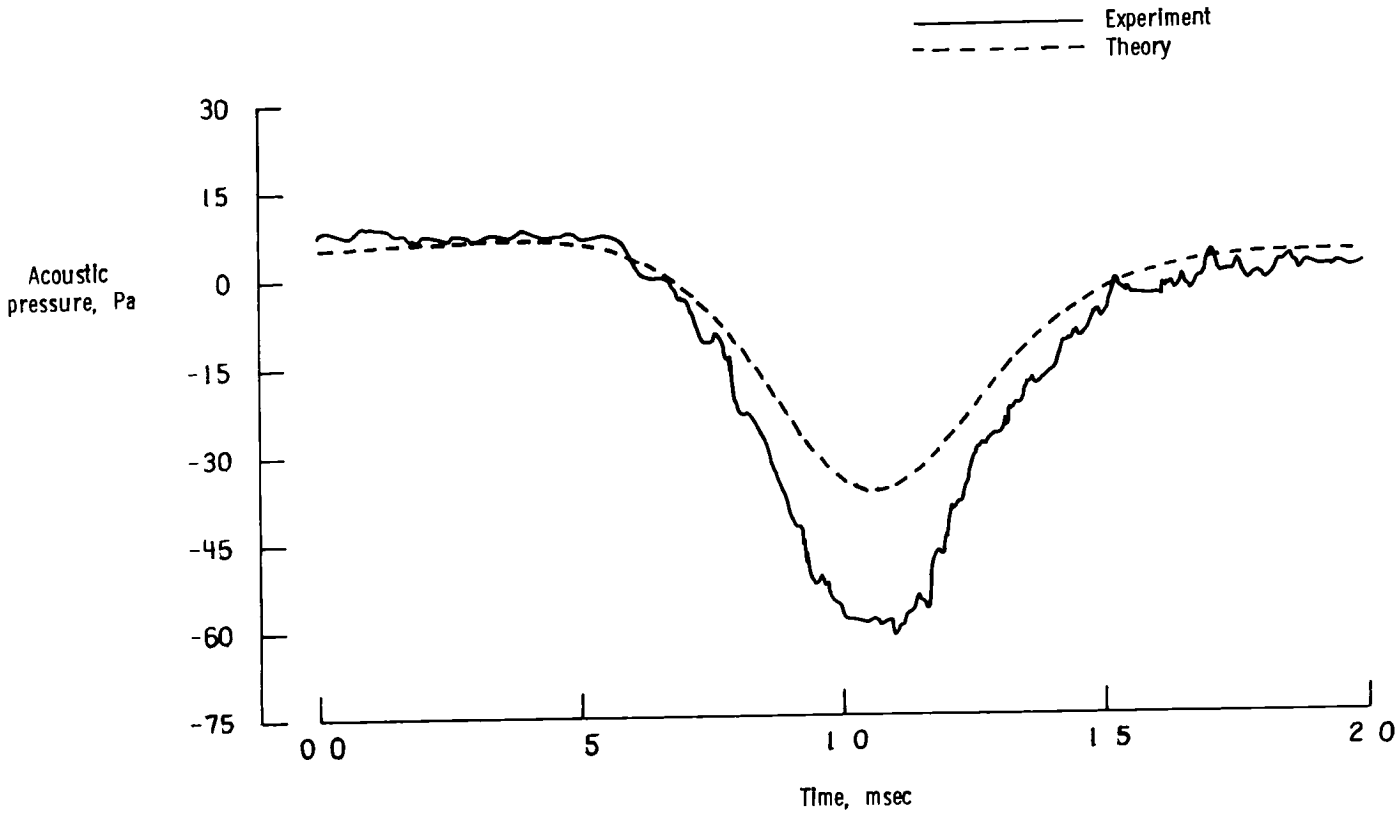

(a) $M_t = 0.80$

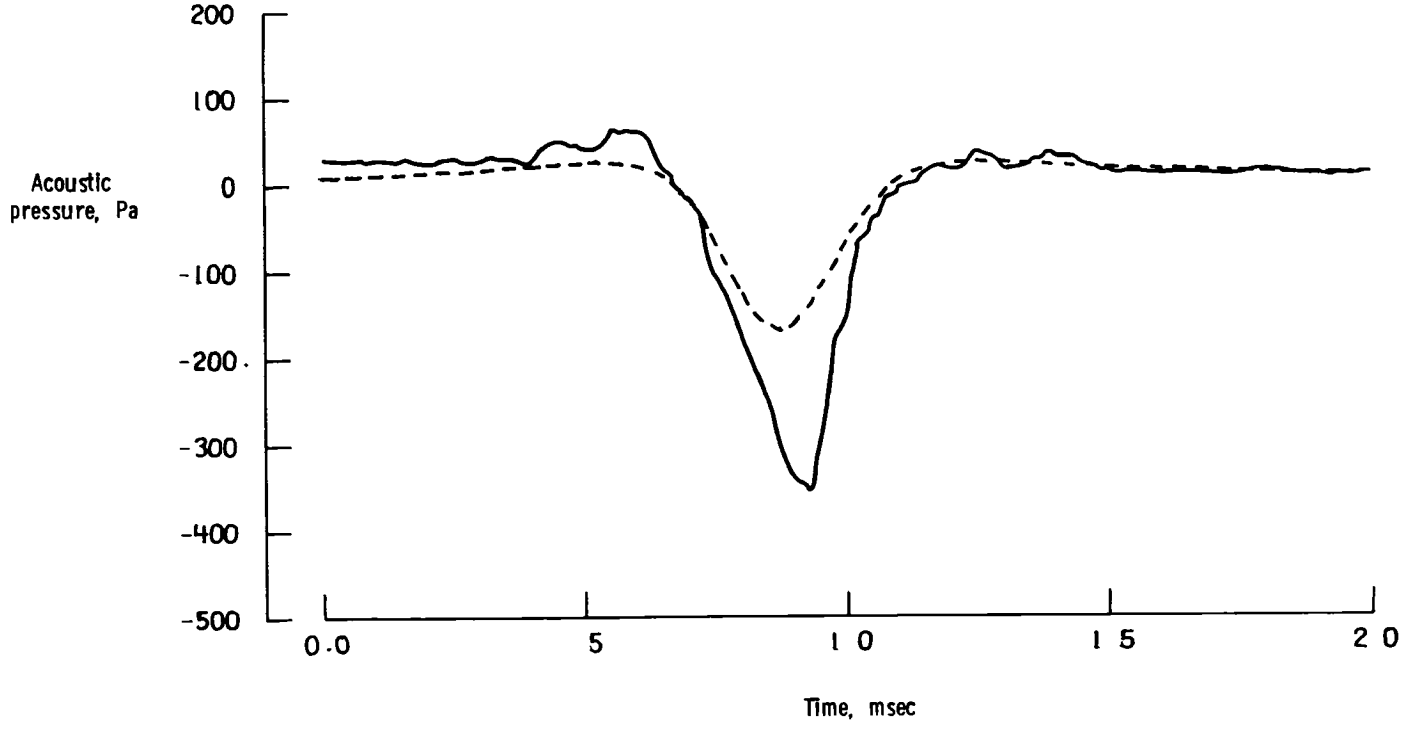

(b) $M = 0.88$

Figure 12. - Comparison of theoretical and experimental pressure signatures in rotor plane at 3 rotor radii from rotor center.

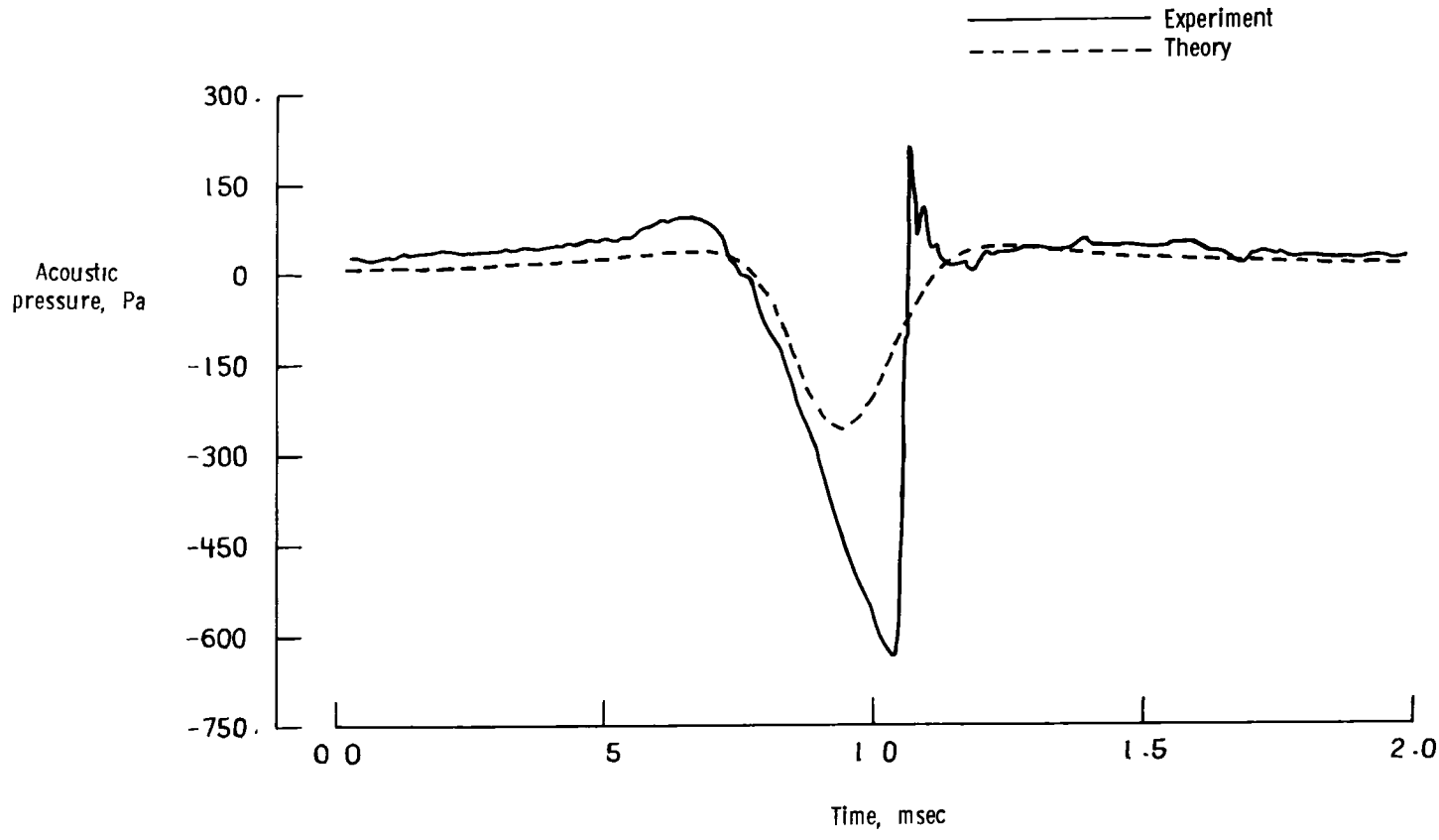

(c) $M_t = 0\ 90$

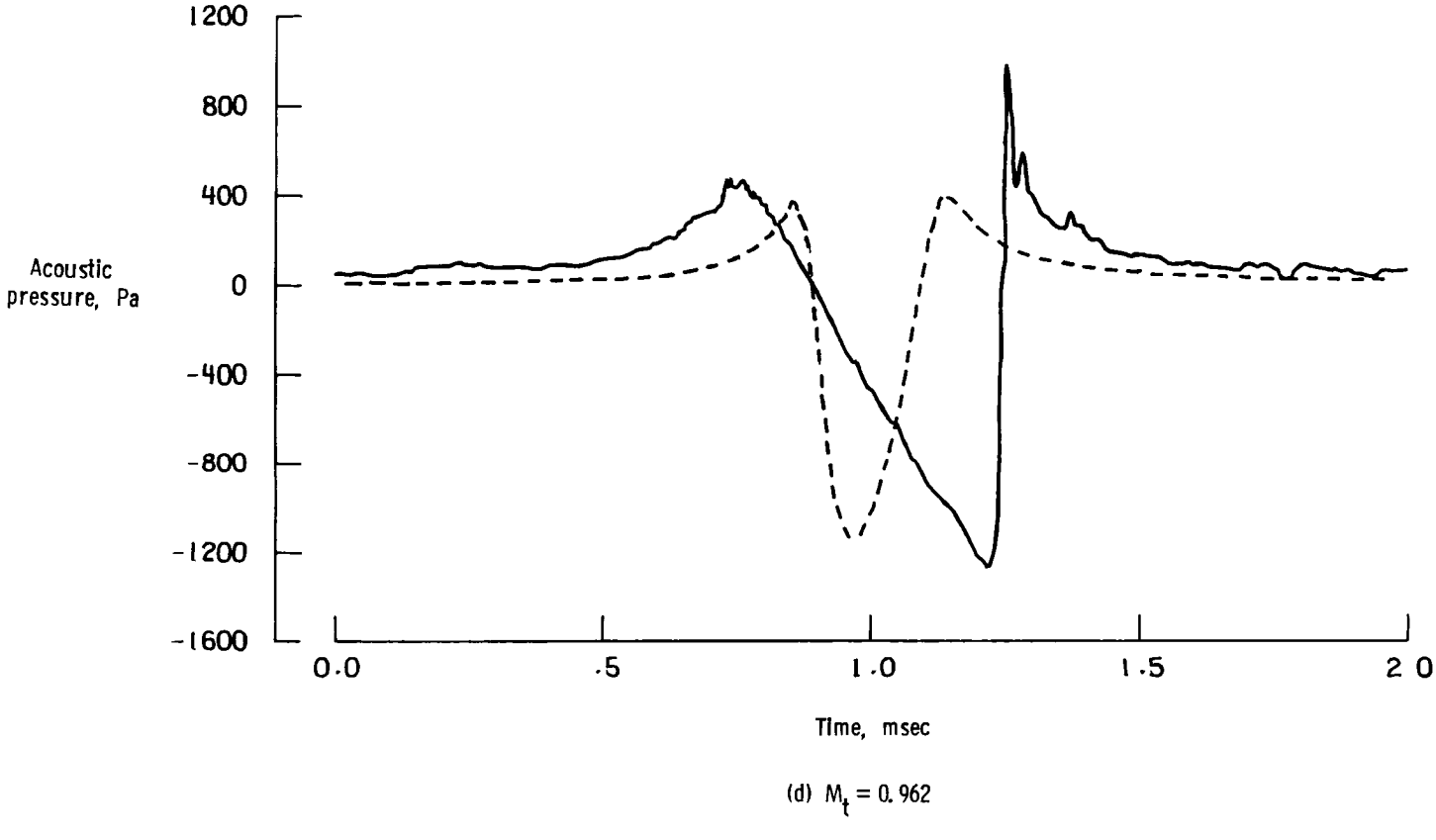

(d) $M_t = 0.962$

Figure 12 - Concluded

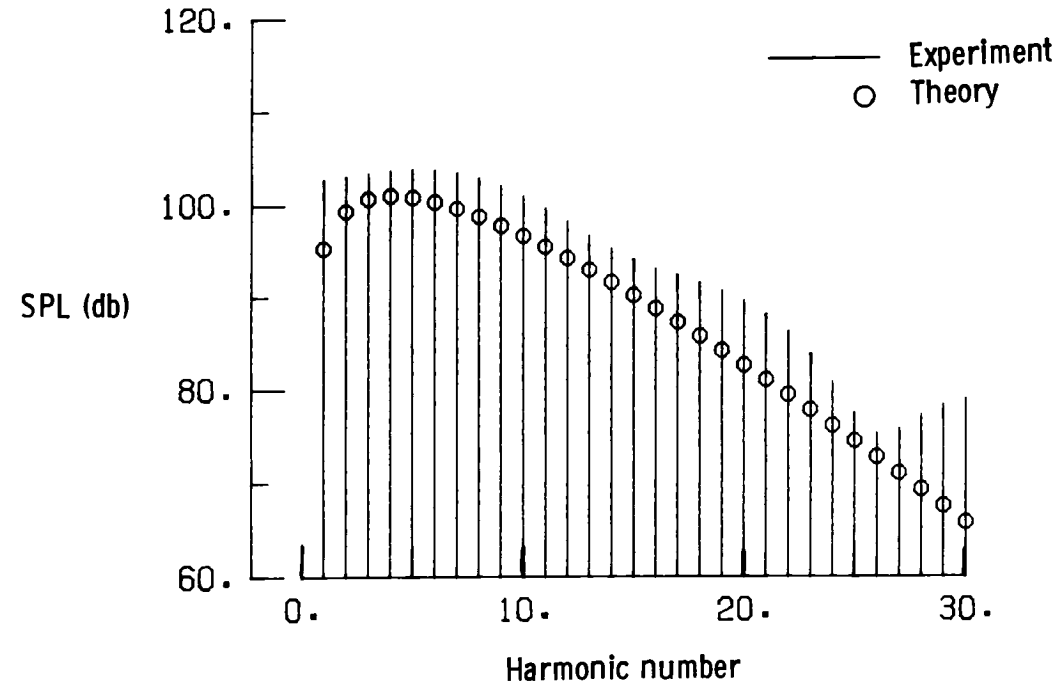

(a) $M_t = 0.80$

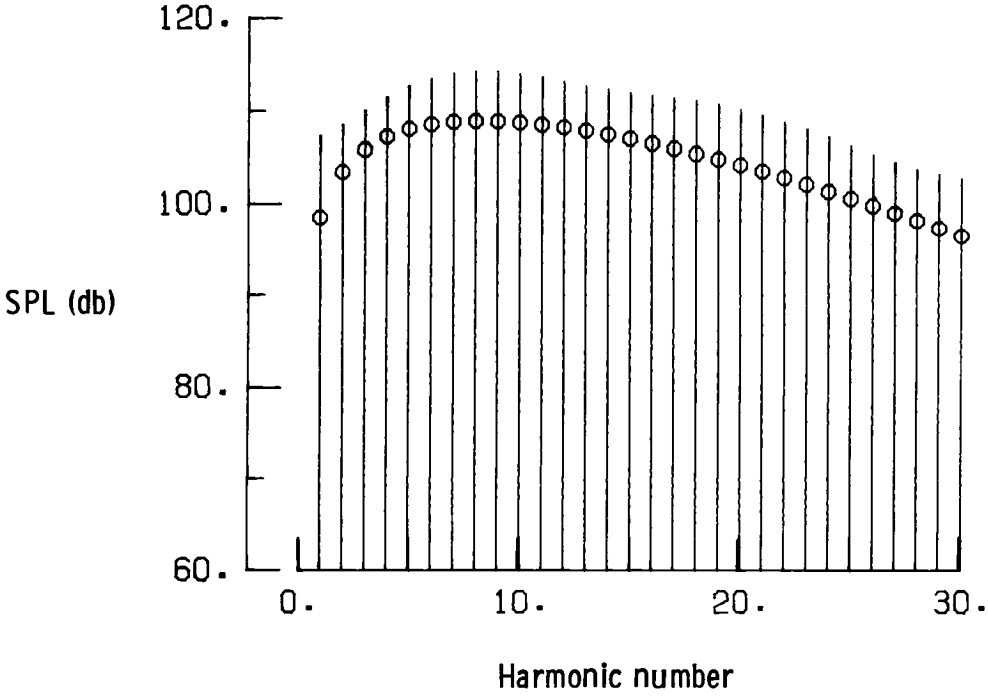

(b) $M_t = 0.88$

Figure 13. - Comparison of theoretical acoustic pressure spectra in rotor plane at 3 rotor radii from rotor center.

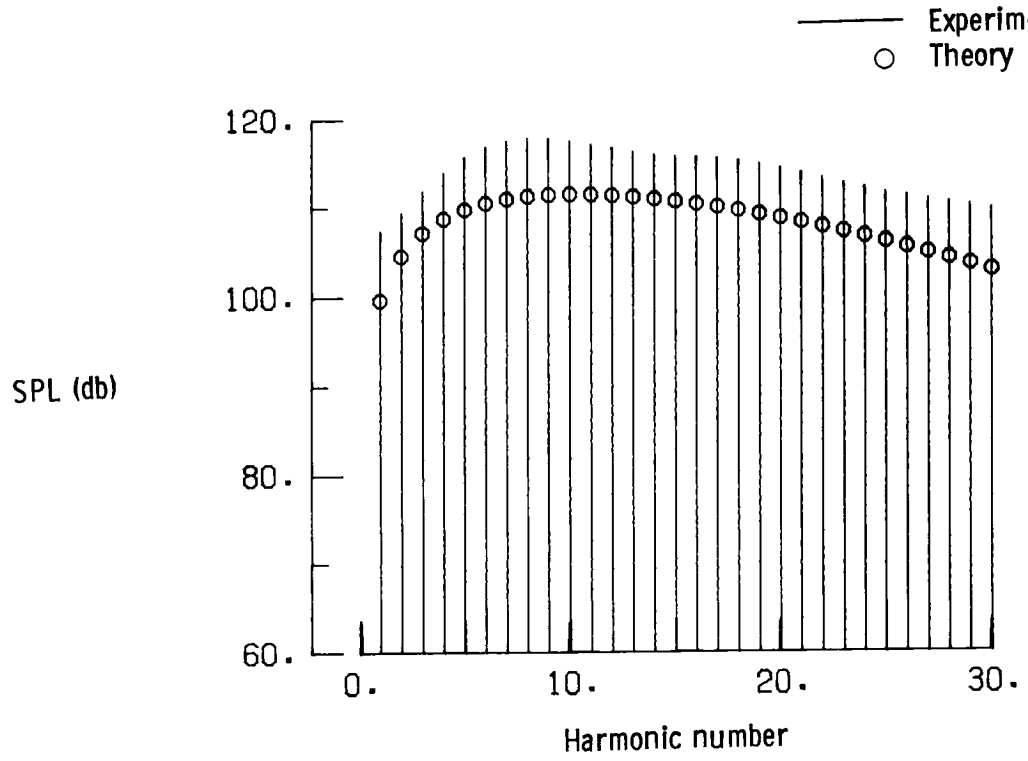

(c) $M_t = 0.90$

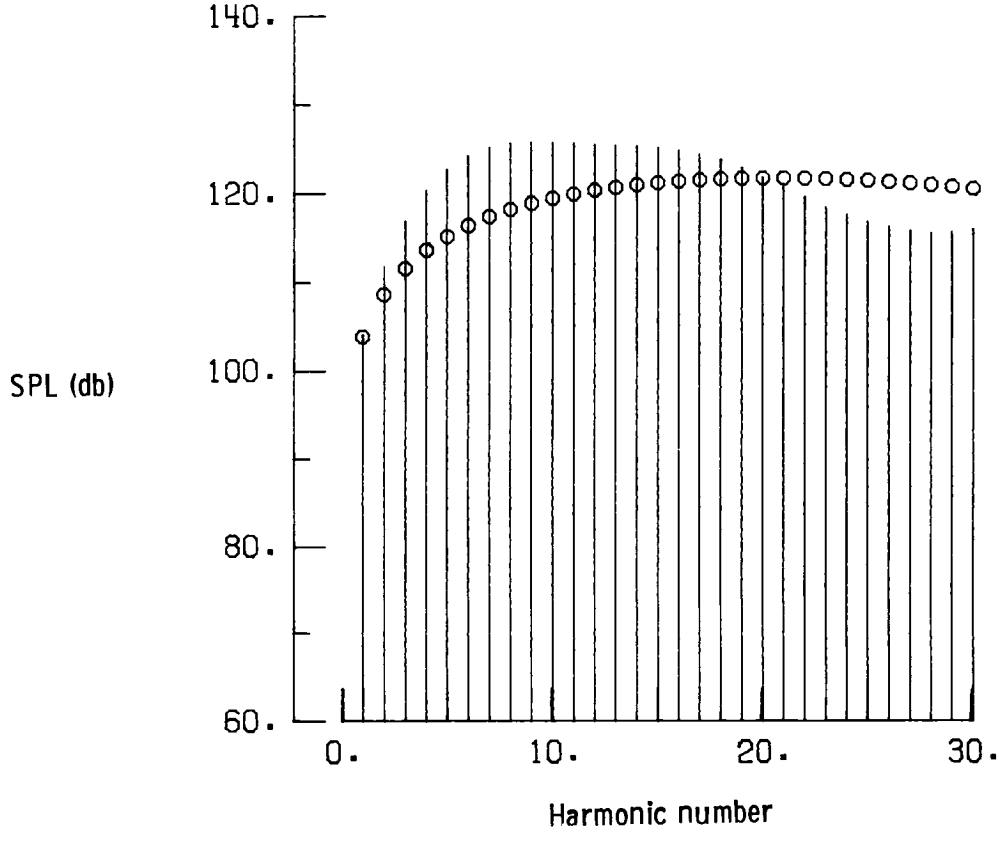

(d) $M_t = 0.962$

Figure 13. - Concluded.

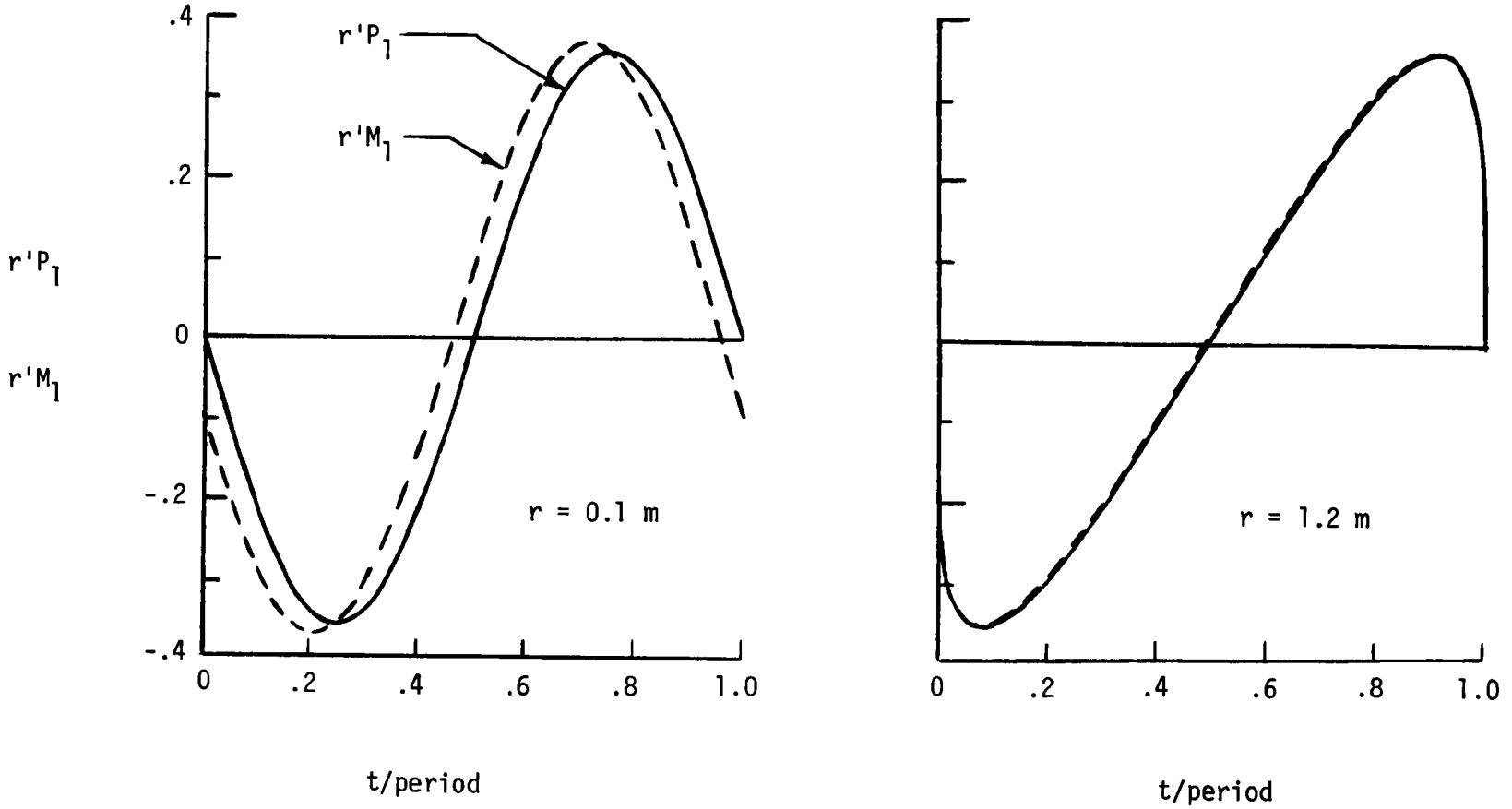

Figure 14.- Time history of pressure and fluid velocity at two distances from the center of an oscillating sphere. a = 0.1 m; ω = 2000 hz.

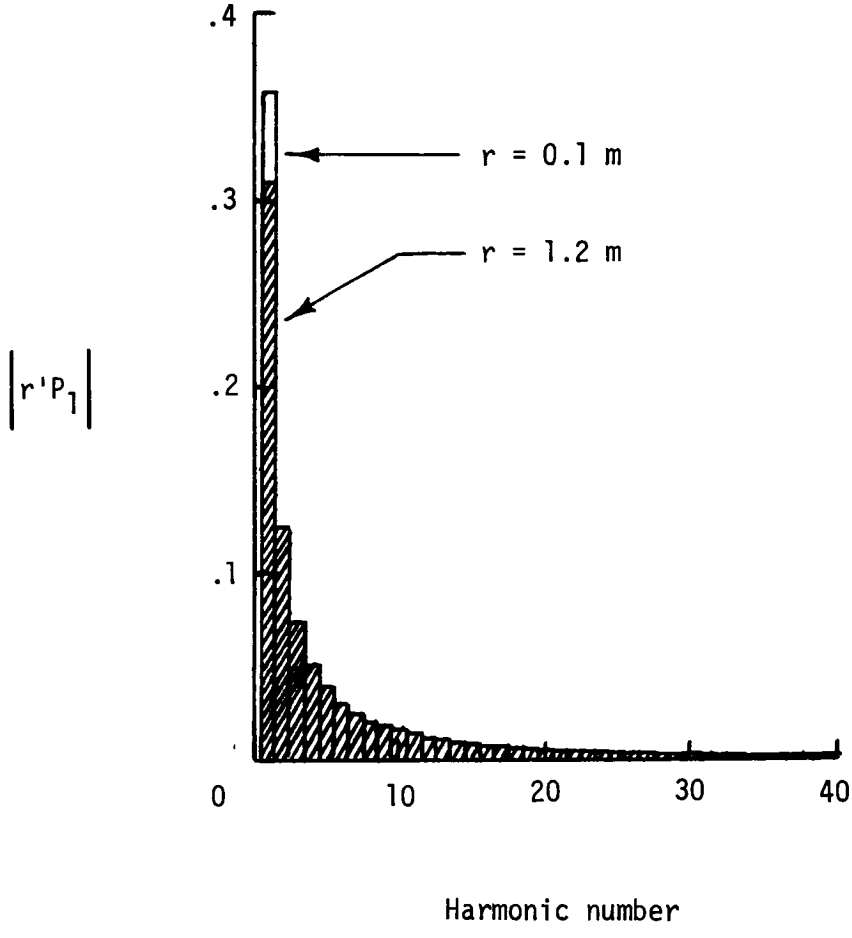

Figure 15.- Amplitude of harmonics of pressure at two distances from the center of an oxcillating sphere. a = 0.1 m; ω = 2000 hz.

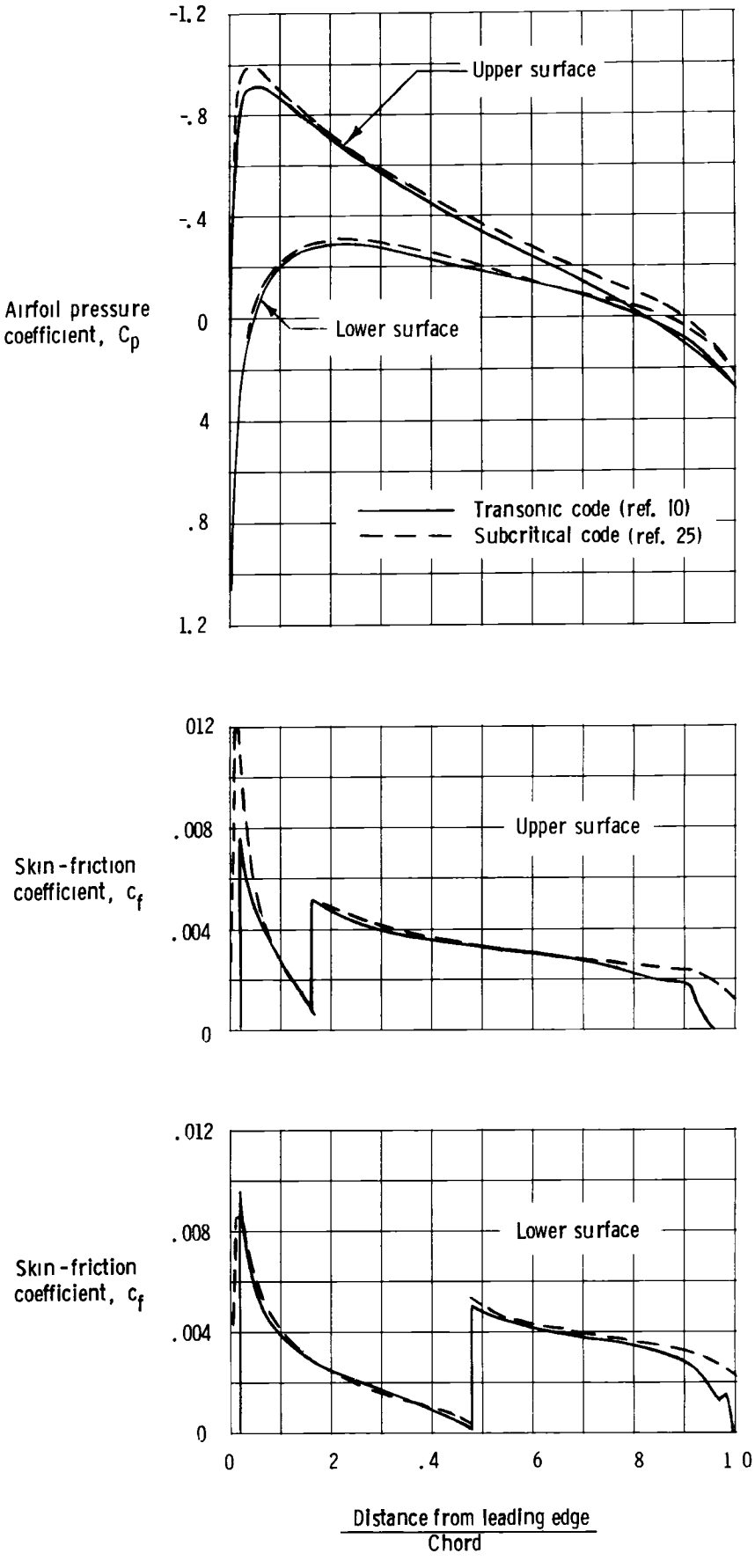

Figure 16. - Comparison of airfoil aerodynamics computed with two methods. NACA 0012 airfoil at $M = 0.6$, $\alpha = 2°$

End of Document